PHILOSOPHICAL TRANSACTIONS A

rsta.royalsocietypublishing.org

Review

Cite this article: Barker B, Humpherys J, Lyng G, Lytle J. 2018 Evans function computation for the stability of travelling waves. *Phil. Trans. R. Soc. A* **376**: 20170184. http://dx.doi.org/10.1098/rsta.2017.0184

Accepted: 13 November 2017

One contribution of 14 to a theme issue 'Stability of nonlinear waves and patterns and related topics'.

Subject Areas:
differential equations, wave motion, computational mathematics

Keywords:
Evans function, travelling waves, stability

Author for correspondence:
Jeffrey Humpherys
e-mail: jeffh@math.byu.edu

Evans function computation for the stability of travelling waves

B. Barker[1], J. Humpherys[1], G. Lyng[2] and J. Lytle[1]

[1]Department of Mathematics, Brigham Young University, Provo, UT 84602, USA
[2]Department of Mathematics and Statistics, University of Wyoming, Laramie, WY 82071, USA

JH, 0000-0003-3981-1217

In recent years, the Evans function has become an important tool for the determination of stability of travelling waves. This function, a Wronskian of decaying solutions of the eigenvalue equation, is useful both analytically and computationally for the spectral analysis of the linearized operator about the wave. In particular, Evans-function computation allows one to locate any unstable eigenvalues of the linear operator (if they exist); this allows one to establish spectral stability of a given wave and identify bifurcation points (loss of stability) as model parameters vary. In this paper, we review computational aspects of the Evans function and apply it to multidimensional detonation waves.

This article is part of the theme issue 'Stability of nonlinear waves and patterns and related topics'.

1. Introduction

Nonlinear travelling waves appear as particular solutions in a wide variety of models of natural phenomena. Important examples include shock waves and detonations in compressible fluid flow [1,2], solitary waves in optics and bodies of water [3,4], migrating population densities in ecology [5], phase transitions in materials [6] and chemotaxis in cell motion [7].

As with any evolutionary system, some notion of stability is necessary to characterize robust phenomena. In the case of travelling waves, stability means that the shape of the wave is steadily maintained as it propagates

THE ROYAL SOCIETY PUBLISHING

forward in time, and that small disturbances in the wave decay away without ill-effect. More precisely, stability in this context means that the perturbed wave converges to a translate of the original unperturbed wave.

The absence of stability, both physically and mathematically, is manifested by sensitivity to small disturbances or perturbations which distort or otherwise alter the state of the system, resulting in either irregular behaviour or a transition to another state. Thus, in this sense, stability is the arbiter of whether a given travelling wave solution is physically viable. In recent years, there have been several developments that have impacted our understanding of travelling wave stability. In particular, a large body of methods built around the Evans function[1] have been developed to attack a diverse variety of problems; see [12–14] for overviews. The Evans function, denoted $D(\lambda)$, is defined as a Wronskian of decaying solutions of the eigenvalue problem $\lambda v = \mathcal{L}v$, as derived from the linearized system $v_t = \mathcal{L}v$. Under fairly general conditions, the Evans function is analytic on an open set containing the closed, deleted[2] right half of the complex plane

$$\Pi = \{z \in \mathbb{C} \mid \mathrm{Re}\lambda \geq 0, \lambda \neq 0\}.$$

In a manner similar to the characteristic polynomial, the roots of the Evans function correspond exactly, both in location and multiplicity, to the eigenvalues of $\mathcal{L}$; see [15] for a rigorous treatment. Thus, by computing the Evans function along contours in Π, winding numbers can be calculated, and one can systematically count and locate its roots (and hence the eigenvalues of $\mathcal{L}$) within. If there are no roots of the Evans function in Π, then the given travelling wave is spectrally stable. In the case of instability, one can produce bifurcation diagrams to illustrate and observe its onset as parameters in the system vary; see [16–18] for illustrative examples.

Given an evolution equation $u_t = \mathcal{F}(u)$, we note that travelling wave solutions $\hat{u}$ moving forward at speed s are equivalent to steady-state solutions in a moving frame $x \to x - st$. In other words, the travelling wave solution $\hat{u}$ is also the steady-state solution of the translated evolution equation $u_t = su_x + \mathcal{F}(u)$. Hence, the linearized behaviour about $\hat{u}$ can be determined by the linear partial differential equation $v_t = \mathcal{L}v := (s\partial_x + D\mathcal{F}(\hat{u}))v$ for the perturbation v. It is natural to examine the corresponding eigenvalue problem $\lambda v = \mathcal{L}v$, where $\mathcal{L} : \mathcal{X} \to \mathcal{X}$ is a densely defined differential operator on a certain Banach space $\mathcal{X}$ of perturbations; see [14,19,20] for details.

We then write the eigenvalue problem as a first-order system of ordinary differential equations (ODEs)

$$W' = A(x;\lambda)W, \quad W \in \mathbb{C}^n, \quad ' = \frac{d}{dx}. \tag{1.1}$$

Assuming that $\hat{u}$ converges exponentially to the constant states $u_\pm$ as $x \to \pm\infty$, it follows that $A(x;\lambda)$ converges exponentially to the constant matrices

$$A_\pm(\lambda) = \lim_{x \to \pm\infty} A(x;\lambda). \tag{1.2}$$

Moreover, if the constant matrices in (1.2) have the same inertia for all $\lambda \in \Pi$, that is if both $A_+(\lambda)$ and $A_-(\lambda)$ can each be split into k growth and $n-k$ decay modes, then one can show that a non-trivial bounded solution of (1.1) corresponds to the intersection of the k-dimensional unstable manifold $U_-(x;\lambda)$ growing from zero at $x = -\infty$ and the $(n-k)$-dimensional stable manifold $S_+(x;\lambda)$ decaying to zero at $x = +\infty$. This intersection can be detected by the vanishing of a certain determinant, and the resulting Evans function is analytic on Π.

Numerically, it is very difficult to integrate the stable and unstable manifolds of (1.1). There are significant issues with stiffness in (1.1) that result from the multi-mode growth and decay rates of the corresponding manifolds. Integrating naively results in a compounding of errors that yields unreliable output. This issue was first remedied by Pego (in the appendix of [21]), who was the first to use the compound-matrix method [22–26] to compute the Evans function. Essentially this method lifts (1.1) into an appropriate wedge-product space where it can be

[1]Developed by J. Evans in his work on the stability of nerve axon equations [8–11].

[2]Because the set of travelling waves solutions is invariant under translations $x \to x + c$, there is always an eigenvalue at $\lambda = 0$, and so we exclude the origin from the closed right-half plane in our definition of spectral stability.

integrated numerically as a single trajectory. This approach was subsequently rediscovered and further developed independently by Brin and colleagues [27–29] and Bridges and colleagues [30,31] a few years later. The compound-matrix method fixes the problems with stiffness, but at the cost of factorial computational complexity. In particular, an n-dimensional system with k and $n-k$ dimensional unstable/stable manifolds at the two endpoints, respectively, becomes an $\binom{n}{k}$-dimensional system of ODEs, which is computationally prohibitive unless n is rather small.

In 2006, Humpherys & Zumbrun [32] proposed a new approach that represents the unstable and stable manifolds using the continuous orthogonalization method of Drury [33] together with a scalar ODE that restores analyticity. This approach, sometimes described as the *polar-coordinate* method, reduces the time required to compute the Evans function to cubic complexity and has been used in many studies (e.g. [18,34,35]). We provide additional details for this method since we use it in the featured study of multidimensional detonations described in §5.

Other clever methods for computing the Evans function have also been considered. Ledoux *et al.* [36] choose an optimal coordinate patch representation for evolving the flow along the underlying Grassmann manifold. Gesztesy *et al.* [37] derive general perturbation expansions for analytically varying Fredholm determinants thus allowing them to avoid computing an Evans function. Lafortune *et al.* [38] evolve the entire flow while monitoring a Wronskian condition and adaptively changing integration tolerances to obtain reasonable results. Barker *et al.* [39] compute the Evans function as a boundary value problem. Methods have also been developed for numerically computing the periodic Evans function [40] and for obtaining a rigorous enclosure of the Evans function [41].

In this paper, we review a number of central computational aspects of the Evans function, and we illustrate them by presenting new computational results for the stability of multidimensional viscous strong detonation waves. In §2, we describe the Evans function. In §3, we give an overview of the computational details including the polar-coordinate and adjoint formulations of the Evans function, how to deal with error bounds in the output, and some best practices for counting and locating roots. Section 4 provides a simple example of the Evans function for viscous shock layers in the isentropic Navier–Stokes equations as initially reported in [42]. We conclude this paper by presenting new Evans function results for planar strong detonations in §5.

2. Theoretical background

We review the construction of the Evans function. Given the eigenvalue problem $\lambda v = \mathcal{L}v$ that comes from linearizing the flow about the travelling wave solution $\hat{u}$ as described above, we write the eigenvalue problem as a first-order system (1.1) and identify an eigenvalue of $\mathcal{L}$ with a non-trivial solution W of (1.1) satisfying $W(\pm\infty) = 0$.

(a) The Evans function

There are three main assumptions for the matrix $A(x;\lambda)$ defined in (1.1). First, we assume for each $\lambda \in \Pi$ that $A_\pm(\lambda)$ are consistently split; that is, they have the same inertia and no eigenvalues on the imaginary axis. More precisely, if $E^{\mathrm{u}}_\pm(\lambda)$ and $E^{\mathrm{s}}_\pm(\lambda)$ are the unstable and stable eigenspaces of $A_\pm(\lambda)$, respectively, we require that $\dim E^{\mathrm{u}}_-(\lambda) = k$ and $\dim E^{\mathrm{s}}_+(\lambda) = n-k$ for some fixed k, $0 < k < n$. Second, we assume that $A(x;\lambda)$ is analytic for $\lambda \in \Pi$, and third that $A(x;\lambda) \to A_\pm(\lambda)$ exponentially in x for each $\lambda \in \Pi$; that is, there exists an $\alpha > 0$ such that

$$A(x;\lambda) = A_\pm(\lambda) + \mathcal{O}(\mathrm{e}^{-\alpha|x|}) \tag{2.1}$$

as $x \to \pm\infty$. In particular, convergence is uniform in λ over compact subsets of $\Pi \cup \{0\}$.

As a result of these three assumptions, a non-trivial bounded solution W of (1.1) exists if and only if the unstable manifold $U_-(x;\lambda)$ at $x = -\infty$ intersects non-trivially with the stable manifold $S_+(x;\lambda)$ at $x = +\infty$. The existence of non-trivial solutions of (1.1) follows from theory of exponential dichotomies, which characterizes the conditional stability of linear systems of ODEs; see [43] for details.

More precisely, the unstable and stable manifolds mentioned above are defined as the sets of initial conditions of (1.1) that flow to zero towards their respective end-states; that is,

$$U_-(x_0;\lambda) = \{W_0 \in \mathbb{C}^n \mid W(x) \to 0 \text{ as } x \to -\infty \text{ where } W(x_0) = W_0\}$$

and

$$S_+(x_0;\lambda) = \{W_0 \in \mathbb{C}^n \mid W(x) \to 0 \text{ as } x \to \infty \text{ where } W(x_0) = W_0\}.$$

Note that $U_-(x;\lambda)$ and $S_+(x;\lambda)$ are subspaces of $\mathbb{C}^n$ having dimension k and $n-k$, respectively. It follows that $\lambda \in \mathbb{C}$ is an eigenvalue of $\mathcal{L}$ if and only if $U_-(0;\lambda) \cap S_+(0;\lambda) \neq \{0\}$.

Let

$$\left.\begin{aligned} W_-(x;\lambda) &= [W_1^-(x;\lambda) \quad \cdots \quad W_k^-(x;\lambda)] \in \mathbb{C}^{n\times k} \\ \text{and} \qquad W_+(x;\lambda) &= [W_{k+1}^+(x;\lambda) \quad \cdots \quad W_n^+(x;\lambda)] \in \mathbb{C}^{n\times(n-k)}, \end{aligned}\right\} \tag{2.2}$$

be matrices whose columns are *analytic bases* of $U_-(x;\lambda)$ and $S_+(x;\lambda)$, respectively. We define the Evans function as

$$D(\lambda) = \det([W_-(x;\lambda) \quad W_+(x;\lambda)])\Big|_{x=0}. \tag{2.3}$$

This is an analytic function whose zeros correspond exactly in location and multiplicity to the eigenvalues of $\mathcal{L}$; see [15] for a rigorous treatment.

Computing the Evans function is rather tricky. Ideally, we would simply integrate (1.1) for some analytic set of basis vectors $W_-(-L;\lambda)$ of the space $U_-(-L;\lambda)$ from $x=-L$ to $x=0$ and similarly integrate some analytic set of basis vectors $W_+(L;\lambda)$ of the space $S_+(L;\lambda)$ backwards from $x=L$ to $x=0$ and then compute (2.3). However, this presents several problems. First, it is not clear how to come up with bases vectors for $U_-(-L;\lambda)$ and $S_+(L;\lambda)$ for even a single value λ. Since the condition that defines $U_-(-L;\lambda)$ and $S_+(L;\lambda)$ is based on their asymptotic convergence to zero, we can prove they exist, but it is hard to accurately identify them numerically. Second, supposing we did have initial basis vectors $W_-(-L;\lambda)$ and $W_+(L;\lambda)$, if we naively integrated (1.1) from $x=\pm L$ to $x=0$ numerically, our results would be garbage. This is due to stiffness inherent in numerically integrating linear multi-mode systems; indeed, the errors in the trajectories will swamp the integration and result in unreliable output. Thirdly, it's also unclear how to choose the bases $W_\pm(\pm L;\lambda)$ to be analytically varying in λ. Since $U_-(x;\lambda)$ and $S_+(x;\lambda)$ are subspaces, any constant multiple of basis vectors are also basis vectors, and therefore there is no reason to assume that $W_\pm(\pm L;\lambda)$ will be analytically varying, not to mention continuous. This feature has to be 'built-in' to the computational method.

To resolve the first issue, we make use of the 'gap lemma' [44,45], which leverages the exponential convergence of $A(x;\lambda)$ to the constant matrices $A_\pm(\lambda)$. Specifically, for fixed λ, choose bases $V_-(\lambda)$ of $E_-^{\mathrm{u}}(\lambda)$ and $V_+(\lambda)$ of $E_+^{\mathrm{s}}(\lambda)$. It follows that

$$W_\pm(x;\lambda) = \mathrm{e}^{A_\pm(\lambda)(x\mp L)}V_\pm(\lambda)(1 + O(\mathrm{e}^{-\alpha|x|})). \tag{2.4}$$

In other words, while we do not know the values of $W_\pm(\pm L;\lambda)$, we do know that they can be well-approximated, when L is sufficiently large, by $W_\pm(\pm L;\lambda) = V_\pm(\lambda)$. Furthermore, we know that the trajectories produced by these approximate initial conditions will give us sufficiently accurate values of the Evans function to where we can rely on its output for winding number calculations; see §3f for details.

The second issue is solved by numerically integrating with the polar-coordinate method, as described in §3b. Other methods exist (e.g. [30,36]), but this approach is arguably the easiest to explain and implement.

The third (and last) issue is resolved by making sure that the basis vectors $V_\pm(\lambda)$ are analytically varying. This is accomplished by using Kato's method, as described in §3d. This makes the Evans function (2.3) analytic and therefore suitable for winding number calculations.

(b) The adjoint formulation

For fixed $\lambda \in \Pi$, if $k > n/2$, it is often advantageous to use the adjoint formulation of the Evans function [46]. Instead of finding the k-dimensional unstable manifold $U_-(x;\lambda)$ of (1.1) at $x = -\infty$, we find the $(n-k)$-dimensional unstable manifold $\tilde{U}_-(x;\lambda)$ of the adjoint ODE $\tilde{W}' = -A(x;\lambda)^*\tilde{W}$ at $x = -\infty$. Denoting the ith column of $\tilde{W}_-(x;\lambda)$ by $\tilde{W}_i(x)$ and the jth column of $W_-(x;\lambda)$ by $W_j(x)$, we note that

$$\begin{aligned}(\tilde{W}_i(x)\cdot W_j(x))' &= \tilde{W}_i(x)\cdot W_j'(x) + (\tilde{W}_i)'(x)\cdot W_j(x)\\ &= \tilde{W}_i^*(x)A(x;\lambda)W_j(x) - \tilde{W}_i^*(x)A(x;\lambda)W_j(x) = 0.\end{aligned}$$

Hence, $\tilde{W}_i(x)\cdot W_j(x) \equiv$ const. and since $\tilde{W}_i(-\infty)\cdot W_j(-\infty) = 0$, we have that $\tilde{W}_i$ and W_j are orthogonal for all x. Hence, $\tilde{W}_-^*(x)W_-(x) = 0$. Now, if

$$\det([W_-(x;\lambda) \quad W_+(x;\lambda)])|_{x=0} = 0,$$

or, equivalently, if there exist non-trivial $u \in \mathbb{C}^k$ and $v \in \mathbb{C}^{n-k}$ such that

$$W_-(0;\lambda)u + W_+(0;\lambda)v = 0,$$

we see that

$$0 = \tilde{W}_-^*(0;\lambda)[W_-(0;\lambda)u + W_+(0;\lambda)v] = \tilde{W}_-^*(0;\lambda)W_+(0;\lambda)v, \tag{2.5}$$

thus

$$\det(\tilde{W}_-^*(x;\lambda)W_+(x;\lambda))|_{x=0} = 0. \tag{2.6}$$

Conversely, if (2.6) holds, then there exists $v \in \mathbb{C}^{n-k}$ such that $\tilde{W}_-(0;\lambda)^*W_+(0;\lambda)v = 0$. But since $W_-(0;\lambda)$ forms a basis for the null space of $\tilde{W}_-(0;\lambda)$ and $W_+(0;\lambda)v$ is in the null space of $\tilde{W}_-(0;\lambda)$, there exists $u \in \mathbb{C}^k$ such that $W_-(0;\lambda)u = W_+(0;\lambda)v$. It follows that

$$\det([W_-(x;\lambda) \quad W_+(x;\lambda)])|_{x=0} = 0.$$

Thus, we define the left-adjoint Evans function to be

$$D(\lambda) = \det(\tilde{W}_-^*(x;\lambda)W_+(x;\lambda))|_{x=0}. \tag{2.7}$$

We may similarly define the right-adjoint Evans function using the adjoint at $x = +\infty$, which we would expect to be advantageous when $k < n/2$. In either case, the polar-coordinate method can be easily adapted to the adjoint formulation of the Evans function; see §3c for details.

3. Computational set-up and details

In this section, we describe the steps required to effectively compute the Evans function. We assume that the evolution equation is linearized and the corresponding eigenvalue problem is cast as a first-order system of ODEs as given in (1.1). We begin by showing how to compute the travelling-wave profiles numerically. Then we describe the polar-coordinate method and how to use the polar-coordinate method for the adjoint formulation of the Evans function. We then explain the initialization process with Kato's method to ensure that the bases for the unstable and stable manifolds are chosen analytically. We briefly examine the kinds of contours one considers when computing, and then we conclude the section with a discussion on how to count and locate the unstable roots of the Evans function and therefore establish whether a given travelling wave is (spectrally) unstable.

(a) Computing the travelling wave

The travelling wave profile is determined by solving a two-point boundary value problem (BVP) on the infinite domain $-\infty < x < \infty$:

$$U'(x) = f(U(x)), \quad U \in \mathbb{R}^N, \quad \lim_{x\to\pm\infty} U(x) = U_\pm \quad \text{and} \quad ' = \frac{\mathrm{d}}{\mathrm{d}x}. \tag{3.1}$$

Fronts and pulses correspond, respectively, to heteroclinic and homoclinic orbits in the N-dimensional phase space, and, in general, this is a task that requires numerical computation. To connect the unstable manifold at $x = -\infty$ to the stable manifold at $x = +\infty$, we use projective boundary conditions $P_\pm(U(\pm L) - U_\pm) = 0$ at $\pm L$, where $P_\pm$ are matrices whose columns are orthogonal vectors that respectively span the orthogonal complements of the spans of $df(U_\pm)$ for L sufficiently large. In other words, we project out the stable manifold at $x = -\infty$ and the unstable manifold at $x = \infty$.

Since the mathematical boundary conditions of (3.1) are at $x = \pm\infty$, and the ODE is autonomous, there is a one-parameter manifold of solutions of (3.1) corresponding to translational invariance; that is, $x \to x + c$. We choose a particular solution by including an additional condition at $x = 0$ called the *centring condition*. A typical approach for a front is to set one of the midpoints of $(U_- + U_+)/2$ to occur at $x = 0$ and a typical approach for a pulse is to require that the derivative of the pulse vanish at $x = 0$. Other conditions can also be specified. Hence, we have conditions at $x = \pm L$ and at $x = 0$, and so we are left with a three-point BVP. A useful technique is to double the size of the N-dimensional system and halve the domain, thus going from the N-dimensional problem

$$U' = f(U), \quad x \in [-L, L], \quad U \in \mathbb{R}^N,$$

to the $2N$-dimensional problem

$$\begin{pmatrix} U \\ V \end{pmatrix}' = \begin{pmatrix} f(U) \\ -f(V) \end{pmatrix}, \quad x \in [0, L],\ U, V \in \mathbb{R}^N.$$

Of course to make this work, one usually needs up to N additional 'matching' conditions $U(0) = V(0)$ to ensure that the solutions are continuous at $x = 0$ and to provide enough boundary conditions. Since the projective, centring and matching conditions all occur at $x = 0$ and $x = L$, we have reduced the problem to a two-point BVP, for which several numerical packages exist (e.g. [47–49]).

A common issue is that the wave speed s or some other system parameter may be unknown. To remedy this, we can add another dimension to the system, for example $s' = 0$. This results in a two-point BVP solver on the $(2N + 1)$-dimensional system

$$\begin{pmatrix} U \\ V \\ s \end{pmatrix}' = \begin{pmatrix} f(U) \\ -f(V) \\ 0 \end{pmatrix}, \quad x \in [0, L],\ U, V \in \mathbb{R}^N,$$

subject to the $(2N + 1)$ boundary conditions. Typically, we need at least as many conditions as we have variables for the two-point boundary value solver packages. The final step is typically an initial guess for the solution as most solvers rely on some kind of Newton-like optimization method, where an initial guess is needed to achieve convergence. For fronts and pulses, typical guesses are the hyperbolic tangent and secant functions, respectively. In some cases, finding a suitable initial guess is too difficult in the parameter regime of interest, and so one instead solves the problem in a simpler regime and then uses continuation to find the solutions in the desired regime; see [17] for details.

(b) The polar-coordinate method

The polar-coordinate method [32] works by computing orthogonal bases for the stable and unstable manifolds using the continuous orthogonalization method of Drury [33] and multiplying

their determinant (evaluated at $x=0$) by a complex function that comes from a certain first-order scalar ODE that restores analyticity. This approach reduces the complexity of Evans function computation to cubic complexity and has been used successfully in many studies (e.g. [16–18,50]). Further improvements and generalizations have since been developed as well (e.g. [36,37]).

Assume for each fixed λ that there exist $k\times k$ and $(n-k)\times(n-k)$ smooth matrix-valued functions $\alpha_-(x;\lambda)$ and $\alpha_+(x;\lambda)$, respectively, such that

$$W_-(x;\lambda)=\Omega_-(x;\lambda)\alpha_-(x;\lambda)\quad\text{and}\quad W_+(x;\lambda)=\Omega_+(x;\lambda)\alpha_+(x;\lambda),\tag{3.2}$$

where $\Omega_\pm^*(x;\lambda)\Omega_\pm(x;\lambda)=I$ for all $x\in\mathbb{R}$. These orthogonal decompositions can be computed with any one of several methods including the Drury method [33], the Davey method [51], QR decomposition [52–55] and the polar decomposition [56,57].

Substituting the decomposition (3.2) into the Evans system (1.1) (and hereafter suppressing the independent variables for convenience) gives

$$\Omega'=A\Omega-\Omega g,\quad \alpha'=g\alpha,\tag{3.3}$$

where the choice of g corresponds to the various methods cited above. A necessary condition to enforce orthogonality in Ω is given by $g+g^*=\Omega^*(A+A^*)\Omega$. We note that the Drury method [33], given by $g=\Omega^*A\Omega$, satisfies this condition and is equivalent to setting $\Omega^*\Omega'=0$. Thus, any change in Ω is orthogonal to the space spanned by the columns of Ω; this choice is also associated with the shortest arc length distance on a Stiefel manifold; see [58] for details. With Drury's method, (3.3) becomes

$$\Omega'=(I-\Omega\Omega^*)A\Omega\tag{3.4a}$$

and

$$\alpha'=(\Omega^*A\Omega)\alpha.\tag{3.4b}$$

Bringing it all together in block matrix form, we have

$$[W_-(x;\lambda)\quad W_+(x;\lambda)]=[\Omega_-(x;\lambda)\quad\Omega_+(x;\lambda)]\begin{bmatrix}\alpha_-(x;\lambda) & 0\\ 0 & \alpha_+(x;\lambda)\end{bmatrix}.$$

Hence by taking the determinant, the Evans function takes the form

$$D(\lambda)=\det([W_-(x;\lambda)W_+(x;\lambda)])|_{x=0}=\gamma_-(0;\lambda)\gamma_+(0;\lambda)\det([\Omega_-(x;\lambda)\quad\Omega_+(x;\lambda)])|_{x=0},$$

where $\gamma_\pm(0;\lambda)=\det\alpha_\pm(0;\lambda)$.

Note that to compute the Evans function, we do not actually need to solve for α; we only need its determinant γ. An appeal to Abel's equation[3] allows us to replace (3.4*b*) with the ODE $\gamma'=\mathrm{tr}(g)\gamma$. Thus we compute the Evans function by solving the system

$$\Omega'=(I-\Omega\Omega^*)A\Omega\tag{3.5a}$$

and

$$\gamma'=\mathrm{tr}(\Omega^*A\Omega)\gamma.\tag{3.5b}$$

For initial conditions, we take the polar decomposition $V_\pm(\lambda)=\Omega_\pm(\pm L;\lambda)\alpha(\pm L;\lambda)$ and then set $\gamma(\pm L;\lambda)=\det\alpha(\pm L;\lambda)$.

Remark 3.1. The scalar ODE (3.5*b*) can be transformed into exponentially weighted coordinates by setting $\gamma(x)=\exp(\mp\mathrm{tr}(\Omega_\pm^*A_\pm\Omega_\pm)x)\tilde\gamma(x)$ and solving

$$\tilde\gamma'=\mathrm{tr}(\Omega^*A\Omega-\Omega_\pm^*A_\pm\Omega_\pm)\tilde\gamma.$$

Thus, when $|x|$ is large, the right-hand side is zero and an adaptive solver can take relatively large steps; this offers a significant speed-up to the solver.

[3]If a system of ODE is $\alpha'(x)=M(x)\alpha(x)$ and the determinant of $\alpha(x)$ is denoted by $\gamma(x)$, then Abel's equation says that $\gamma'(x)=\mathrm{tr}(M(x))\gamma(x)$.

Remark 3.2. It is conventional wisdom in the continuous orthogonalization literature that Drury's method is numerically unstable and one should use Davey's method [51] or any one of several other methods studied in the literature (e.g. [59,60]). However, Drury's method is stable when integrating the unstable manifold in forward time or the stable manifold in backward time, which is what is done in Evans function computation with the polar-coordinate method; see [61] for details.

(c) Adjoint version of the polar-coordinate method

As described in §2b, we may define the Evans function by using the adjoint formulation. We begin with the decomposition $\tilde{W}_-(x;\lambda) = \tilde{\Omega}_-(x;\lambda)\tilde{\alpha}_+(x;\lambda)$, where $\tilde{\Omega}_-(x;\lambda)$ is an continuous $n \times (n-k)$ matrix with orthonormal columns and $\tilde{\alpha}_-(x;\lambda)$ is a continuous $(n-k)\times(n-k)$ matrix. Again, we do not need to integrate $\alpha(x;\lambda)$, rather we only need its determinant; that is, $\tilde{\gamma}_+^*(x;\lambda) = \det\tilde{\alpha}_-(x;\lambda)^*$. The matrix $\tilde{\Omega}_-(x;\lambda)$ and the scalar function $\tilde{\gamma}_+^*(x;\lambda)$ are obtained by integrating from $x=-L$ to $x=0$ the ODE (3.5) where $A(x;\lambda)$ is replaced with $-A(x;\lambda)^*$.

When using the left adjoint formulation (2.7), the Evans function takes the form

$$\begin{aligned} D(\lambda) &= \det(\tilde{W}_-^*(x;\lambda)W_+(x;\lambda))|_{x=0} \\ &= \det(\tilde{\alpha}_-^*(x;\lambda)\tilde{\Omega}_-^*(x;\lambda)\Omega_+(x;\lambda)\alpha_+(x;\lambda))|_{x=0} \\ &= \tilde{\gamma}_-^*(0;\lambda)\gamma_+(0;\lambda)\det(\tilde{\Omega}_-^*(x;\lambda)\Omega_+(x;\lambda))|_{x=0}. \end{aligned}$$

Remark 3.3. As with the regular construction of the Evans function, one should also employ the use of exponentially weighted coordinates for the left-adjoint formulation, as described in remark 3.1.

(d) Initialization with Kato's method

In order for the Evans function $D(\lambda)$ to be analytic in λ, the bases $V_\pm(\lambda)$ at the numerical end states need to be chosen analytically. Recall from §2 that there are analytic eigenspaces $E_-^{\mathrm{u}}(\lambda)$ and $E_+^{\mathrm{s}}(\lambda)$ describing how the unstable and stable subspaces of $A_\pm(\lambda)$ evolve as λ varies. Let $\{v_j^-\}_{j=1}^k$ and $\{v_j^+\}_{j=k+1}^n$ be, respectively, bases for $E_-^{\mathrm{u}}(\lambda_0)$ and $E_+^{\mathrm{s}}(\lambda_0)$ for some fixed λ_0. By using the method of Kato [62, p. 99] (see also [29,30,63]), we find the (unique) analytically varying bases $\{v_j^-(\lambda)\}_{j=1}^k$ and $\{v_j^+(\lambda)\}_{j=k+1}^n$ yielding analytically varying matrices $V_\pm(\lambda)$ in (2.4).

Specifically, the analytic basis vectors must satisfy the ordinary differential equation

$$\frac{\mathrm{d}}{\mathrm{d}\lambda}v_j^\pm(\lambda) = [P_\pm'(\lambda), P_\pm(\lambda)]v_j^\pm(\lambda) \tag{3.6}$$

subject to the initial condition $v_j^\pm(\lambda_0) = v_j^\pm$, where $[\cdot,\cdot]$ represents the commutator and $P(z)$ denotes the analytic projection onto the range of its appropriate subspace, along its complementary subspace. We can numerically approximate (3.6), following [64], by using the second-order scheme

$$v_j^\pm(\lambda_{j+1}) = v_j^\pm(\lambda_j) + \tfrac{1}{2}(P_\pm(\lambda_{j+1}) - P_\pm(\lambda_j))(P_\pm(\lambda_{j+1}) + P_\pm(\lambda_j))v_j^\pm(\lambda_j),$$

where $\{\lambda_j\}_{j=1}^m$ is a discretization of the contour being computed.

(e) Executing the shooting method

In order to use the Evans function to definitively determine the existence of eigenvalues, one must have a bound on the modulus of permissible unstable spectra thus reducing the problem to looking for zeros of the Evans function on a compact subset $\Lambda \subset \{z \in \mathbb{C} \mid \mathrm{Re}\, z \geq 0\}$. By the assumptions made in §2, the Evans function D is analytic on Λ. According to the argument principle, if the Evans function does not vanish on the boundary $\partial\Lambda$, which is assumed to be

a Jordan curve, then we may determine the number of zeros n of D in Λ by a winding number computation,

$$n = \frac{1}{2\pi \mathrm{i}} \oint_{z \in \partial\Lambda} \frac{D'(z)}{D(z)}\, \mathrm{d}z. \tag{3.7}$$

As $0 \in \partial\Lambda$, and since the derivative of the travelling wave profile is an eigenfunction with eigenvalue zero corresponding to translational invariance of the profile [65], the winding number contour integral cannot be computed on $\partial\Lambda$ without modification. If the region on which the Evans function is analytic includes a ball centred at the origin, then Λ can be modified to make zero an interior point. As long as the resulting winding number matches the multiplicity of the zero eigenvalue, then no unstable eigenvalues exist. When one must exclude a small ball around the origin from Λ in order to compute the winding number due to an eigenvalue at zero, Λ typically takes the form of the right half of an annulus centred at the origin.

Remark 3.4. If the system is a conservation law in one spatial dimension; for example, the constant viscosity system $U_t + f(U)_x = BU_{xx}$, then the eigenvalue problem

$$\lambda U - sU' + (Df(\hat{U})U)' = BU'', \tag{3.8}$$

($\hat{U}$ is the profile) can be expressed in integrated coordinates [42]. More precisely, by letting $U = V'$ and integrating in x, the resulting eigenvalue problem

$$\lambda V - sV' + Df(\hat{U})V' = BV''$$

has the same eigenvalues (with the same multiplicity) as (3.8), except that the zero corresponding to translational invariance is removed. We note that for multi-dimensional planar waves in conservation laws, the eigenvalue corresponding to zero can be removed from the Evans function by using balanced flux coordinates [66]. In these scenarios, Λ is often taken to be the right half of a circle with centre at the origin.

(f) Rouché bounds and winding numbers

Once Λ is appropriately determined, we proceed to the computation of the Evans function. The Evans function defined in (2.3) uses the manifolds $W_\pm(x;\lambda)$, which satisfy (1.1) and asymptotically approach zero tangent to an analytic bases $V_\pm(\lambda)$ of the unstable and stable subspaces of $A_\pm$, respectively. The numerically approximated matrix functions $W_\pm^L(x;\lambda)$ solve the initial value problem (1.1) with initial condition $W_\pm^L(\pm L;\lambda) = V_\pm(\lambda)$. One then defines

$$E_L(\lambda) := \det([W_-^L(x;\lambda) \quad W_+^L(x;\lambda)])|_{x=0}.$$

It follows that $E_L(\lambda)$ is an analytic function, but in general the roots of E_L and D are not exactly the same due to numerical and approximation error. However, Rouché's theorem guarantees that E_L and D have the same number of roots inside Λ as long as

$$|D(\lambda) - E_L(\lambda)| < |E_L(\lambda)| \tag{3.9}$$

for all $\lambda \in \partial\Lambda$. If $D(\lambda)$ does not vanish on $\partial\Lambda$, one may guarantee that equation (3.9) holds by taking L sufficiently large. Indeed, one may show by a contraction mapping that $W_\pm^L(\pm L;\lambda)/|W_\pm^L(\pm L;\lambda)|$ approaches $W_\pm(\pm L;\lambda)/|W_\pm(\pm L;\lambda)|$ uniformly in Λ at exponential rate as $L \to \infty$ [42], thus it follows that $W^L(0;\lambda)/|W^L(0;\lambda)| \to W(0;\lambda)/|W(0;\lambda)|$ at exponential rate. Hence, for fixed $\lambda_0 \in \Lambda$ and $\lambda \in \Lambda$,

$$\frac{D(\lambda_0)}{E_L(\lambda_0)} E_L(\lambda) \to D(\lambda)$$

uniformly at exponential rate as $L \to \infty$ [61].

Finally, we must appropriately choose the mesh along $\partial\Lambda$ on which we compute the Evans function. The image $E(\partial\Lambda)$ should not vary in argument by more than π between mesh points to ensure that the correct sign is attributed to the change in argument. Alternatively, the relative distance between mesh points on the image should be less than one. In practice, it is common

to require the relative error be smaller, like 0.2, in order to minimize the chance that the Evans function has undetected rapid variation between mesh points. One may then determine the winding number of $E(\partial\Lambda)$ by summing the signed changes in angle between consecutive mesh points.

(g) Root finding with the method of moments

Once it is determined that a contour contains roots of the Evans function, one may want to locate those roots and track them as parameters in the system vary. Root finding can be performed in various ways [60,67,68]. If the root is on the real axis, then $D(\lambda)$ is real-valued and any standard root solver should work reasonably well; for example, the secant method. For complex roots, Muller's method has been used with reasonable success.

A nice approach for root finding follows the *method of moments* as described in [17,68,69]. This follows from the *argument principle* in complex analysis. Assume that f is analytic inside and on a simple positively oriented closed curve Λ. If f is non-zero on Λ and $z_1, \ldots, z_n$ are the roots of $f(z)$ inside Λ, then the pth moment of f about z_* (which is usually the origin) is

$$M_p(z_*) = \frac{1}{2\pi \mathrm{i}} \oint_\Lambda \frac{(z - z_*)^p f'(z)}{f(z)} = \sum_{k=1}^{n} (z_k - z_*)^p. \tag{3.10}$$

By computing the first $n+1$ moments, we locate the n roots precisely as long as n is small (due to poor conditioning). For example, $M_0(0) = n$ gives the number of roots inside Λ; that is, $M_0(0)$ is the winding number, $M_1(0) = z_1 + z_2 + \cdots + z_n$ gives the sum of the roots, and $M_2(0) = z_1^2 + z_2^2 + \cdots + z_n^2$ is the sum of the squares of the roots. If many roots are present, it is a good idea to slice up the domain with smaller contours and repeat the process (e.g. [18]). Numerically, the integral (3.10) can be computed with any reasonable method of numerical integration along the contours.

Remark 3.5. To track a single root as parameters in the system vary, one can integrate around a contour that contains exactly one root, then the first-order moment returns an approximate location of that root, and doing this for increasingly small contours yields increasingly accurate results. This is a rather inefficient approach for tracking roots. A more efficient and elegant approach is to use continuation and follow the Evans solution; see [70] for details.

4. One-dimensional example: isentropic Navier–Stokes shocks

As our first example, we consider the p-system with real viscosity. This system is also known as the isentropic compressible Navier–Stokes equations in one spatial dimension. In Lagrangian coordinates, these equations read

$$v_t - u_x = 0, \quad u_t + p(v)_x = \left(\frac{u_x}{v}\right)_x, \tag{4.1}$$

where v is the specific volume, u is the velocity and $p(v)$ is the pressure law which we assume to satisfy $p(v) = a_0 v^{-\gamma}$, $a_0 > 0$ and $\gamma \geq 1$.

(a) Travelling waves

We seek travelling-wave solutions to (4.1) with end states $(v_\pm, u_\pm)$, satisfying $0 < v_+ < v_-$. Equivalently, by translating $(x,t) \to (x - st, t)$, we consider stationary solutions of

$$v_t - s v_x - u_x = 0, \quad u_t - s u_x + (a_0 v^{-\gamma})_x = \left(\frac{u_x}{v}\right)_x.$$

Rescaling by $(x,t,v,u) \to (-\varepsilon s x, \varepsilon s^2 t, v/\varepsilon, -u/(\varepsilon s))$, where $\varepsilon = v_-$ yields

$$v_t + v_x - u_x = 0, \quad u_t + u_x + (a v^{-\gamma})_x = \left(\frac{u_x}{v}\right)_x, \tag{4.2}$$

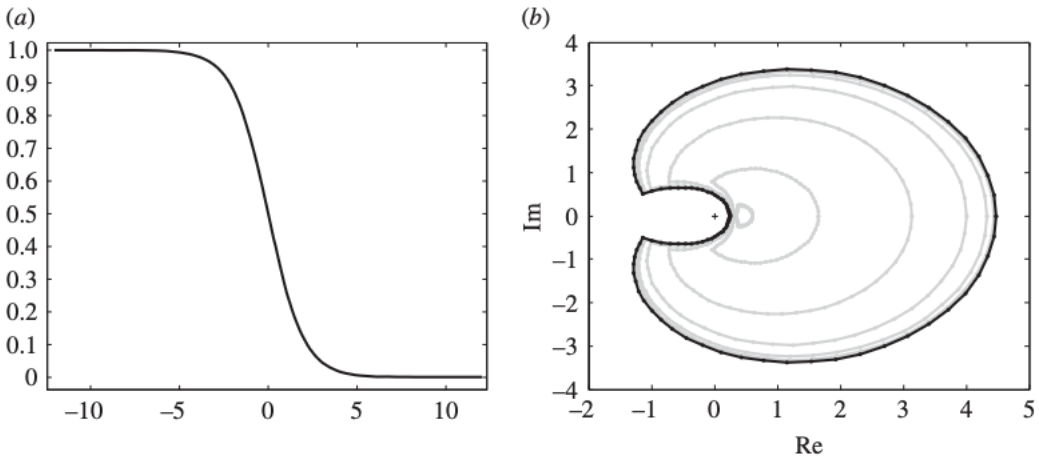

Figure 1. The profile (*a*) and Evans function output (*b*) for the *p*-system as $v_+ \to 0$.

where $a = a_0 \varepsilon^{-\gamma-1} s^{-2}$. The profile $(\hat{u}, \hat{v})$ thus satisfies,

$$\hat{v}' - \hat{u}' = 0, \quad \hat{u}' + (a\hat{v}^{-\gamma})' = \left(\frac{\hat{u}'}{\hat{v}}\right)',$$

with boundary conditions $(\hat{v}(\pm\infty), \hat{u}(\pm\infty)) = (v_\pm, u_\pm)$, where $0 < v_+ < v_- = 1$. Simplifying, we obtain

$$\hat{v}' + (a\hat{v}^{-\gamma})' = \left(\frac{\hat{v}'}{\hat{v}}\right)'. \tag{4.3}$$

Integrating (4.3) from $-\infty$ to x, we obtain the profile equation

$$\hat{v}' = \hat{v}(\hat{v} - 1 + a(\hat{v}^{-\gamma} - 1)). \tag{4.4}$$

Clearly $v_- = 1$ is an equilibrium for (4.4). The necessary (for the existence of a connection) condition that v_+ also be an equilibrium leads to the following definition of a:

$$a = -\frac{v_+ - 1}{v_+^{-\gamma} - 1} = v_+^{\gamma} \frac{1 - v_+}{1 - v_+^{\gamma}}.$$

Since the profile equation (4.4) is scalar, the existence of travelling-wave solutions is straightforward to prove, and these solutions can be easily approximated using the technique described in §3a; see the left-hand panel in figure 1*a*.

(b) Eigenvalue equation

We linearize (4.2) about the profile $(\hat{v}, \hat{u})$ to find the eigenvalue problem,

$$\lambda v + v' - u' = 0 \quad \text{and} \quad \lambda u + u' - \left(\frac{h(\hat{v})}{\hat{v}^{\gamma+1}} v\right)' = \left(\frac{u'}{\hat{v}}\right)', \tag{4.5}$$

where $h(\hat{v}) = -\hat{v}^{\gamma+1} + a(\gamma - 1) + (a + 1)\hat{v}^{\gamma}$. As in remark 3.4, we can change to integrated coordinates, $(u, v) \to (u', v')$, yielding

$$\lambda v + v' - u' = 0 \quad \text{and} \quad \lambda u + u' - \frac{h(\hat{v})}{\hat{v}^{\gamma+1}} v' = \frac{u''}{\hat{v}}. \tag{4.6}$$

We then write (4.6) as a first-order system, and we obtain the Evans system $W' = A(x;\lambda)W$ where

$$A(x;\lambda) = \begin{pmatrix} 0 & \lambda & 1 \\ 0 & 0 & 1 \\ \lambda\hat{v} & \lambda\hat{v} & f(\hat{v}) - \lambda \end{pmatrix} \quad \text{and} \quad W = \begin{pmatrix} u \\ v \\ v' \end{pmatrix}, \quad ' = \frac{\mathrm{d}}{\mathrm{d}x}. \tag{4.7}$$

Here, $f(\hat{v}) = \hat{v} - \hat{v}^{-\gamma}h(\hat{v})$, with h as before.

In figure 1, we observe the numerical profile and the Evans function output as $v_+ \to 0$. We note that in this limit, the Evans function approaches a limiting contour also pictured in figure 1. Humpherys *et al.* discovered this limiting behaviour numerically which led them to prove stability analytically in the limiting case [50] demonstrating the power of employing the Evans function to study shock wave stability; see [42] for additional information.

Remark 4.1. We remark that the numerical investigations in this paper were performed by via Stablab: a Matlab-based numerical library for Evans function computation [71]. This specific example considered above is built in to the package.

5. Multidimensional example: planar viscous detonation waves

Detonation waves are particular, shock-like solutions of models for chemically reacting mixtures of compressible gases. Generally speaking, they are known to have delicate stability properties. Here, to illustrate the computational techniques described in this paper, we present new Evans-function computations for planar detonation-wave solutions of system (5.1).

(a) Background

Classical models for detonation phenomena typically neglect diffusive effects (viscosity, heat conductivity and species diffusion) [18,72]; that is, these effects are treated as negligible relative to the advective and reactive effects that are believed to principally drive behaviour.[4] The paradigmatic example is the well-known Zel'ldovich–von Neumann–Döring (ZND) model developed in 1940s; this model consists of the first-order (inviscid) equations for conservation of mass, momentum and energy coupled to an equation modelling the progress of the chemical reaction. In this model, detonation waves have the structure of an ideal (invisicid) gas-dynamical shock which compresses the gas, heating it and initiating a chemical reaction. The stability program for detonation waves in the ZND setting was initiated by Erpenbeck [73] in the 1960s, and a variety of authors have continued and built on that program in the following years (e.g. [74]).

More recently, there has been a growing effort to incorporate diffusive effects into the models and to understand their impact on the existence and behaviour of solutions. Indeed, as noted by Powers & Paolucci [75], diffusive length scales are the same order of magnitude as included reaction length scales so that any logically consistent model must include both effects. For example, Majda [76] proposed a scalar model for detonation waves that incorporated the second-order effects, and he conjectured that his simplified model—intended to retain the most basic coupling between the nonlinear motion of the gas (shock waves) and the chemical reaction—might exhibit the kind of stability/bifurcation behaviour known to belong to the physical system. His question has recently been answered in the negative [77,78], but see the related work of Faria *et al.* [79].

Around the same time, Gardner [80] used Conley index techniques to prove the existence of travelling-wave solutions (viscous detonation profiles) for the Navier–Stokes equations; see also [81] for an alternative proof. The Evans-function program for the stability of viscous detonation waves was initiated by Lyng & Zumbrun [82,83] (see also [77,78,84–86]) and computational Evans-function techniques were first applied in the physical setting by Barker *et al.* [18] Notably, this study led to the discovery of a previously unknown phenomenon—termed *viscous*

[4]We refer to detonation waves in models which feature second-order diffusive effects as 'viscous detonation waves'.

Table 1. Navier–Stokes variables and parameters.

ρ	density
p	pressure
$\mathbf{u} = (u_1, \ldots, u_d)^{\mathsf{T}}$	fluid velocity
T	temperature
$\tilde{e}$	specific internal energy
z	mass fraction of reactant
μ, η	viscosity coefficients
κ	heat conductivity
β	species diffusion
k	reaction rate
q	heat release

hyperstablization; that is, in the large-activation-energy limit, there is a return to stability as unstable eigenvalues retreat from the right half plane. At a spectral level, this behaviour is completely distinct from that of the ZND model. Here, we extend these calculations to the multidimensional setting. This extension results in a substantial increase in computational effort. In particular, after linearizing about a planar strong detonation wave, we take the Fourier transform in the transverse spatial directions. This leads to a first-order eigenvalue equation of the form

$$W' = A(x_1; \lambda, \tilde{\xi})W,$$

where x_1 is the direction of propagation, $\lambda \in \mathbb{C}$ is dual to time and $\tilde{\xi} \in \mathbb{R}^{d-1}$ is dual to the transverse spatial directions. The goal then, is to use the numerical techniques described in this review to search the half space $\{z \in \mathbb{C} \mid \mathrm{Re}\lambda > 0\} \times \mathbb{R}^{d-1}$ for zeros of the associated Evans function. We begin by introducing the Navier–Stokes equations for a reacting mixture of gases in d-space dimensions. For our computations, we shall take $d = 2$. In contrast to the computations reported in [18], we work in Eulerian coordinates. This introduces additional difficulties with the computation; see [87] for a detailed discussion of this point. For a reacting gas mixture with a one-step exothermic reaction in d space dimensions, the equations in Eulerian coordinates are

$$\rho_t + \mathrm{div}(\rho \mathbf{u}) = 0, \tag{5.1a}$$

$$(\rho u_j)_t + \mathrm{div}(\rho u_j \mathbf{u}) + p_{x_j} = \mu \Delta u_j + (\mu + \eta)\mathrm{div}(\mathbf{u}_{x_j}), \quad j = 1, \ldots d, \tag{5.1b}$$

$$(\rho \tilde{E})_t + \mathrm{div}[(\rho \tilde{E} + p)\mathbf{u}] = \Delta\left(\kappa T + \mu \frac{|\mathbf{u}|^2}{2}\right) + \mu \mathrm{div}((\nabla \mathbf{u})\mathbf{u}) + \eta \mathrm{div}((\mathrm{div}\mathbf{u})\mathbf{u}) + \mathrm{div}(q\rho\beta\nabla z) \tag{5.1c}$$

and

$$(\rho z)_t + \mathrm{div}(\rho z \mathbf{u}) = \mathrm{div}(\rho\beta\nabla z) - k\rho z\varphi(T). \tag{5.1d}$$

Here, we denote time by t and the spatial coordinates by $\mathbf{x} = (x_1, \ldots, x_d)$. The other labels are given in table 1.

This system has $(d + 3)$ unknowns $(\rho, \mathbf{u}, T, z)$. In (5.1c) $\nabla \mathbf{u}$ is the Jacobian matrix of the velocity vector with respect to the spatial variables. We write

$$\tilde{E} = \tilde{e} + \frac{|\mathbf{u}|^2}{2}, \quad \tilde{e} = e + qz,$$

and we take the simplest possible equations of state; that is, we suppose that

$$p = \Gamma\rho e, \quad e = c_v T,$$

where Γ is the Gruneisen constant and c_v is the specific heat at constant volume. Finally, we assume that the ignition function φ will have the form

$$\varphi(T) = \begin{cases} \exp\left(-\dfrac{E_A}{[c_v(T - T_{ig})]}\right) & \text{if } T \geq T_{ig}, \\ 0 & \text{otherwise,} \end{cases}$$

where E_A is the activation energy and T_{ig} is the ignition temperature. Given the simple, linear relationship between e and T, we sometimes find it convenient to write the ignition function as a function of e, with $\breve{\varphi}(e) = \varphi(T)$.

Henceforth, we write $\mathbf{u} = (u, v)$, $\mathbf{x} = (x, y)$. After straightforward manipulations, system (5.1) can then be written as

$$\rho_t + (\rho u)_x + (\rho v)_y = 0, \tag{5.2a}$$

$$(\rho u)_t + (\rho u^2 + p)_x + (\rho uv)_y = (2\mu + \eta)u_{xx} + \mu u_{yy} + (\mu + \eta)v_{xy}, \tag{5.2b}$$

$$(\rho v)_t + (\rho uv)_x + (\rho v^2 + p)_y = \mu v_{xx} + (2\mu + \eta)v_{yy} + (\mu + \eta)u_{yx}, \tag{5.2c}$$

$$\begin{aligned}(\rho E)_t + (\rho uE + up)_x + (\rho vE + vp)_y = {} & (\kappa T_x + (2\mu + \eta)uu_x + \mu v(v_x + u_y) + \eta uv_y)_x \\ & + (\kappa T_y + (2\mu + \eta)vv_y + \mu u(v_x + u_y) + \eta vu_x)_y \\ & + qk\rho z\varphi(T)\end{aligned} \tag{5.2d}$$

and

$$(\rho z)_t + (\rho uz)_x + (\rho vz)_y = (\rho\beta z_x)_x + (\rho\beta z_y)_y - k\rho z\varphi(T), \tag{5.2e}$$

where $E = \tilde{E} - qz = e + u^2/2 + v^2/2$. The next step is to rescale; for completeness, details about the rescaling are posted in appendix Aa.

(b) Travelling waves

We now look for a travelling wave solution

$$(\rho, u, v, e, z)(x, y, t) = (\hat{\rho}, \hat{u}, \hat{v}, \hat{e}, \hat{z})(x - st).$$

By Galilean invariance, we may consider standing profiles ($s = 0$). Evidently, such waves satisfy

$$(\hat{\rho}\hat{u})' = 0, \tag{5.3a}$$

$$(\hat{\rho}\hat{u}^2)' + (\Gamma\hat{\rho}\hat{e})' = (2\mu + \eta)\hat{u}'', \tag{5.3b}$$

$$(\hat{\rho}\hat{u}\hat{v})' = \mu\hat{v}'', \tag{5.3c}$$

$$(\hat{\rho}\hat{u}\hat{E} + \hat{u}\Gamma\hat{\rho}\hat{e})' = \frac{\kappa\hat{e}''}{c_v} + (2\mu + \eta)(\hat{u}\hat{u}')' + \mu(\hat{v}\hat{v}')' + qk\hat{\rho}\hat{z}\breve{\varphi}(\hat{e}) \tag{5.3d}$$

and

$$(\hat{\rho}\hat{u}\hat{z})' = (\hat{\rho}\beta\hat{z}')' - k\hat{\rho}\hat{z}\breve{\varphi}(\hat{e}). \tag{5.3e}$$

From (5.3*a*), we conclude that the mass flux $m := \hat{\rho}\hat{u}$ is constant along the profile. Thus, (5.3*c*) simplifies to $m\hat{v}' = \mu\hat{v}''$, whose only bounded solution is $\hat{v} \equiv$ constant. By an additional coordinate change if necessary, we may assume $\hat{v} = 0$. Further details are given in appendix Ab, from which we have $\hat{\rho} = 1/\hat{u}$. Then setting $\hat{\zeta} = -\hat{\rho}\beta\hat{z}'$ and using (5.4*a*) in the derivation of (5.4*b*), we obtain the first-order system for profiles:

$$\hat{u}' = (2\mu + \eta)^{-1}((\hat{u} - 1) + \Gamma(\hat{u}^{-1}\hat{e} - e_-)), \tag{5.4a}$$

$$\hat{e}' = \nu^{-1}\left((\hat{e} - e_-) - \frac{(\hat{u} - 1)^2}{2} + \Gamma e_-(\hat{u} - 1) + q(\hat{\zeta} + \hat{z} - 1)\right), \tag{5.4b}$$

$$\hat{\zeta}' = \beta^{-1} u\zeta - k\hat{u}^{-1}\hat{z}\check{\varphi}(\hat{e}) \tag{5.4c}$$

and

$$\hat{z}' = -\beta^{-1}\hat{u}\hat{\zeta}. \tag{5.4d}$$

Here, we have used the shorthand $\nu = \kappa/c_v$. Thus, the first step in the computational process will be to approximate solutions of (5.4) that connect the given end states. A necessary condition for a connection is that the end states must be equilibria for (5.4). This leads to the Rankine–Hugoniot jump conditions. We note that when $q = 0$ the profile equations (5.4) reduce to the Navier–Stokes profile equations, with $e_- < e_+$ [88]. This corresponds to end states $z_- = 1$, $z_+ = 0$, and a leftward moving travelling wave. The jump conditions are then easily computed to be

$$(u_+ - 1) + \Gamma(u_+^{-1}e_+ - e_-) = 0, \tag{5.5a}$$

$$(e_+ - e_-) - \frac{(u_+ - 1)^2}{2} + \Gamma e_-(u_+ - 1) + q(\zeta_+ + z_+ - 1) = 0, \tag{5.5b}$$

$$\beta^{-1}u_+\zeta_+ - ku_+^{-1}z_+\check{\varphi}(e_+) = 0 \tag{5.5c}$$

and

$$-u_+\zeta_+ = 0. \tag{5.5d}$$

Since $\zeta_+ = -\beta z_+'/u_+ = 0 = z_+$, equations (5.5c,d) are trivially satisfied.

(c) Computation of the travelling wave

We approximate the wave profiles numerically as described in §3a. The associated Jacobian is given by

$$D_U f = \begin{pmatrix} (2\mu+\eta)^{-1}(1-\Gamma u^{-2}e) & (2\mu+\eta)^{-1}\Gamma u^{-1} & 0 & 0 \\ \nu^{-1}(1-u+\Gamma e_-) & \nu^{-1} & \nu^{-1}q & \nu^{-1}q \\ \beta^{-1}\zeta + ku^{-2}z\check{\varphi}(e) & -ku^{-1}z\check{\varphi}'(e) & \beta^{-1}u & -ku^{-1}\check{\varphi}(e) \\ -\beta^{-1}\zeta & 0 & -\beta^{-1}u & 0 \end{pmatrix}, \tag{5.6}$$

which we use to improve the performance of the boundary value solver. The end states, needed for the projective boundary conditions, are as follows. We have $z_- = 1$ and $z_+ = 0$ are the end states for the mass fraction of the reactant, $u_- = 1$ from the rescaling given in appendix Ab, e_+ and u_+ depend on the variables e_-, Γ and q as determined from the Rankine–Hugoniot conditions, and $\zeta_\pm = 0$ because z has constant end states and $u_\pm \neq 0$.

Substituting $(u_\pm, e_\pm, \zeta_\pm, z_\pm)$ into the Jacobian (5.6), we find that there are two growth and two decay modes at $x = +\infty$ and three growth and one centre mode at $x = -\infty$. Requiring the detonation to approach its end states orthogonal to the centre mode at $x = -\infty$ and to the growth modes at $x = +\infty$ leads to three projective conditions at $x = \pm\infty$. Let P_g and P_c be matrices whose columns are bases for the growth eigenspace at $x = +\infty$ and the centred eigenspace at $x = -\infty$. The boundary conditions for the detonation profiles are

$$P_g^*(U(1) - (u_+, e_+, \zeta_+, z_+)^{\mathrm{T}}) = 0, \tag{5.7}$$

$$P_c^*(V(1) - (u_-, e_-, \zeta_-, z_-)^{\mathrm{T}}) = 0, \tag{5.8}$$

$$U(0) - V(0) = 0 \tag{5.9}$$

and

$$U_1(0) = c, \tag{5.10}$$

where c is the constant $c = (U_1(-\infty) + U_1(+\infty))/2$.

The system parameters for the profile are $\Gamma, (2\mu+\eta), \nu, k, q, \beta, E_A$ and e_-. We note that Evans function computation requires both viscous parameters μ and η, rather than the single

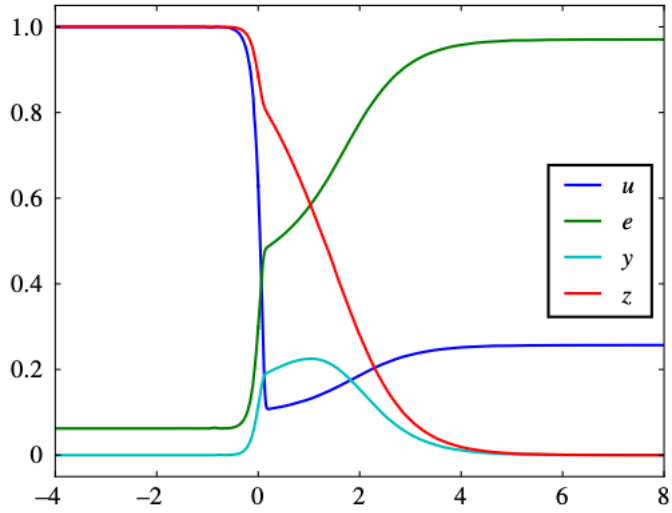

Figure 2. A left-moving travelling wave solution (strong detonation) of (5.1) in Eulerian coordinates, with activation energy $E_A = 2.7$, $(2\mu + \eta) = 0.1$, $e_- = 0.0623$, $\Gamma = 0.2$ and $q = 0.623$. This is the same profile computed in [18], although computed in Eulerian coordinates and oriented towards the left.

parameter $(2\mu + \eta)$ required for the wave profile. An approximation of a profile is shown in figure 2.

(d) The Evans system

The linearized eigenvalue problem may be written in the form $W' = A(x;\lambda,\xi)W$ where $W = [w_1, \tilde{w}_2, w_3, \tilde{w}_4, w_5, u, v, e, z]^{\mathrm{T}}$ and the matrix $A(x;\lambda,\xi)$ is given by

$$\begin{pmatrix}
-\lambda\hat{\rho} & 0 & 0 & 0 & 0 & -\lambda\hat{\rho}^2 & i\xi\hat{\rho} & 0 & 0 \\
-\hat{u}_x & 0 & 0 & 0 & 0 & \lambda\hat{\rho} + \mu\xi^2 & 0 & 0 & 0 \\
-i\xi\hat{p} & 0 & 0 & 0 & 0 & -i\xi\hat{p}\hat{\rho} & \lambda\hat{\rho} + \tilde{\mu}\xi^2 & i\xi\Gamma\hat{\rho} & 0 \\
-\hat{e}_x + \hat{z}f_2 & -\hat{u}_x & 0 & 0 & 0 & \hat{\rho}\hat{z}f_2 & i\xi f_1 & f_4 & -f_2 \\
-\hat{\rho}\hat{z}f_3 & 0 & 0 & 0 & 0 & -\hat{\rho}^2\hat{z}f_3 & i\xi\hat{\rho}\hat{z} & k\hat{\rho}\hat{z}\breve{\varphi}'(\hat{e}) & \hat{\rho}(\beta\xi^2 + f_3) \\
-\tilde{\mu}^{-1}\hat{p} & \tilde{\mu}^{-1} & 0 & 0 & 0 & \tilde{\mu}^{-1}(1 - \hat{p}\hat{\rho}) & -i\tilde{\mu}^{-1}\xi\tilde{\eta} & \tilde{\mu}^{-1}\Gamma\hat{\rho} & 0 \\
0 & 0 & \mu^{-1} & 0 & 0 & -i\mu^{-1}\xi\tilde{\eta} & \mu^{-1} & 0 & 0 \\
0 & 0 & 0 & \nu^{-1} & 0 & (\hat{p} - \tilde{\mu}\hat{u}_x)/\nu & 0 & \nu^{-1} & 0 \\
\hat{z}_x - \hat{u}\hat{z}/\beta & 0 & 0 & 0 & \beta^{-1}\hat{u} & \hat{\rho}\hat{z}_x & 0 & 0 & \beta^{-1}\hat{u}
\end{pmatrix}. \tag{5.11}$$

A sketch of the derivation of $A(x;\lambda,\xi)$ is given in appendix Ad. Here $\lambda \in \mathbb{C}$ is dual to time, and the real frequency parameter ξ arises from a Fourier transform in the y-direction.

The 9×9 Evans matrix (5.11) provides a first-order formulation of the linearized eigenvalue problem. And, with the profile in hand, this is precisely the framework described in §3. Unstable detonations in the multidimensional RNS equations correspond to values of (λ,ξ) with $\mathrm{Re}\lambda > 0$ for which there are non-trivial bounded solutions W of

$$W' = A(x;\lambda,\xi)W. \tag{5.12}$$

A non-trivial bounded solution W must grow along the four-dimensional unstable eigenspace of $A_-(\lambda,\xi)$ near $x = -\infty$, and decay along the five-dimensional stable eigenspace of $A_+(\lambda,\xi)$ near $x = +\infty$. We use the adjoint, polar-coordinate method described above to compute $D(\lambda,\xi)$.

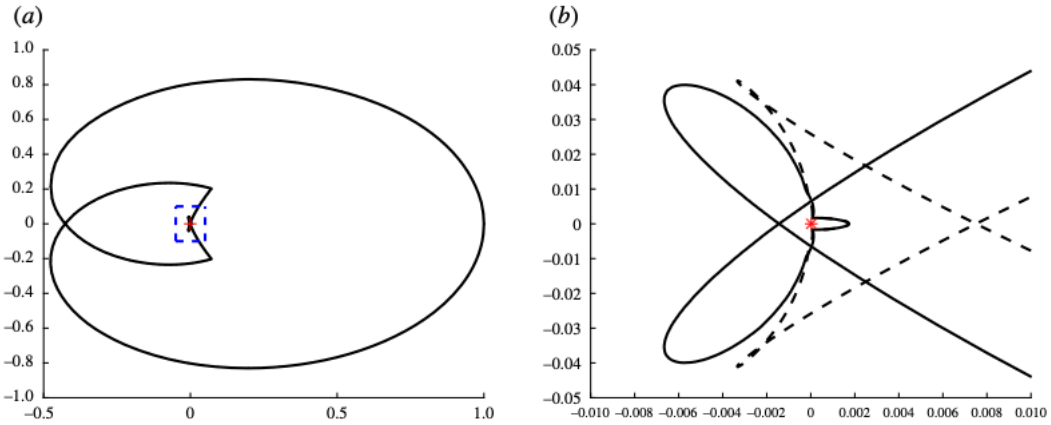

Figure 3. In (*a*), we show the Evans function output for $E_A = 2.7$ on a semicircular contour of radius $R = 0.1$. The inset in (*a*) is magnified in (*b*), where it is easy to see that the winding number changes between $E_A = 2.7$ (solid) and $E_A = 2.8$ (dotted) as a Hopf bifurcation occurs. The other independent parameters are $\xi = 0, e_- = 0.0623, \Gamma = 0.2$ and $q = 0.623$. (Online version in colour.)

(e) Parameter values

For our numerical computations, we set $\mu = \eta = 1/30$, $\beta = 0.1$, $T_{ig} = 0.06641$, and $c_v = 1$. To better compare our results with those in [18], we have chosen k as a function of activation energy E_A. This choice of k regulates the scale length of the reaction, thereby simplifying the solution of the detonation profiles. After setting $\Gamma = 0.2$, $q = 0.623$ and $e_- = 0.0623$, parameters $e_+ = 0.9706$, $u_+ = 0.2569$ are determined by the Rankine–Hugoniot condition.

Detonations are known to experience a cascade of Hopf-like bifurcations at higher values of Imλ as activation energy increases. Our experiments have focused on the smallest pair of eigenvalues as they enter the right half-plane, and eventually return and restabilize. Our parameters of interest are activation energy E_A and the joint parameter ν. The first experiment (figure 3) describes these instabilities as E_A varies between 1.6 and 7.1 with ν fixed. The second experiment fixes E_A and allows ν to vary. This helps us observe the nature of the unstable manifold of eigenvalues present in the multidimensional RNS system; see [18] for comparison (figure 4).

(f) Fixed ν and varying activation energy

For $\nu = 0.1$, we allowed E_A to vary from 1.6 to 7.1 and tracked the first pair of eigenvalues seen crossing into the right half-plane. Since $\xi = 0$ corresponds to the standard 1D RNS Evans function, we were able to verify our results by comparing with those found in [18]. In both systems ($\xi = 0$) instability occurs around $E_A = 2.7$ and the system restabilizes around $E_A = 7.1$. Those eigenvalues also restabilize as ξ increases. Because instabilities in planar detonations correspond to a location λ in the right half-plane and a Fourier frequency ξ, varying activation energy E_A defines a manifold of instabilities (Reλ, Imλ, ξ).

(g) Fixed activation energy with varying ν

These experiments focus on the effect of increasing heat conductivity on the smallest pair of unstable eigenvalues, for several fixed values of activation energy. In general, as heat conductivity increases the unstable pair of eigenvalues returns to the left half-plane and restabilize. This effect is illustrated in figure 5 by plotting the Evans function output on a semicircular contour with radius 0.4 in the right half-plane. As the heat conductivity increases from $\nu = 0.1$ to 0.8, the

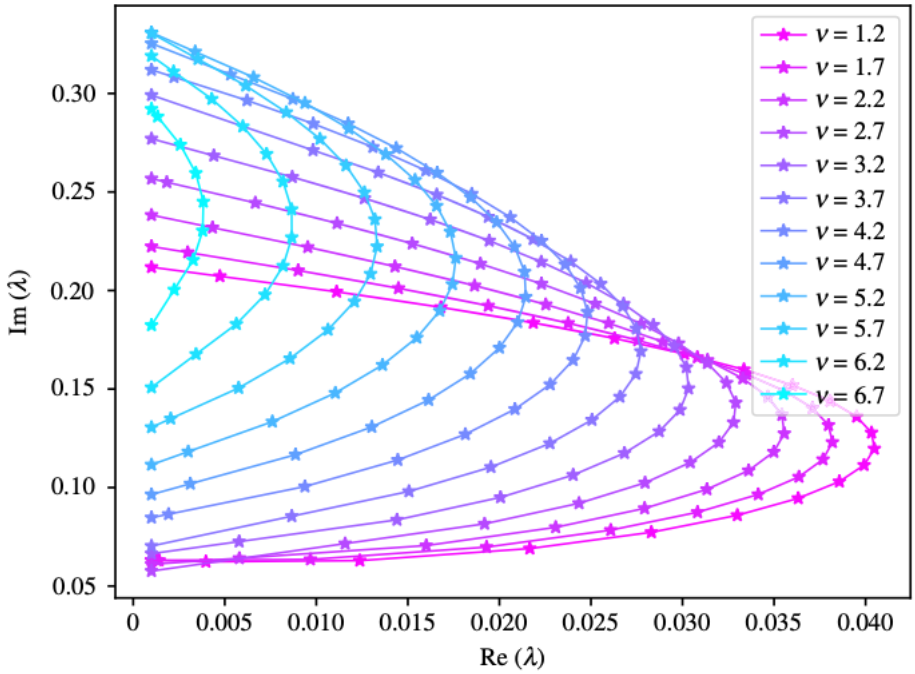

Figure 4. Unstable eigenvalues as heat conductivity ν varies. Each line is parametrized by Fourier frequency ξ. Eigenvalues return to the left half-plane and restabilize as ν increases.

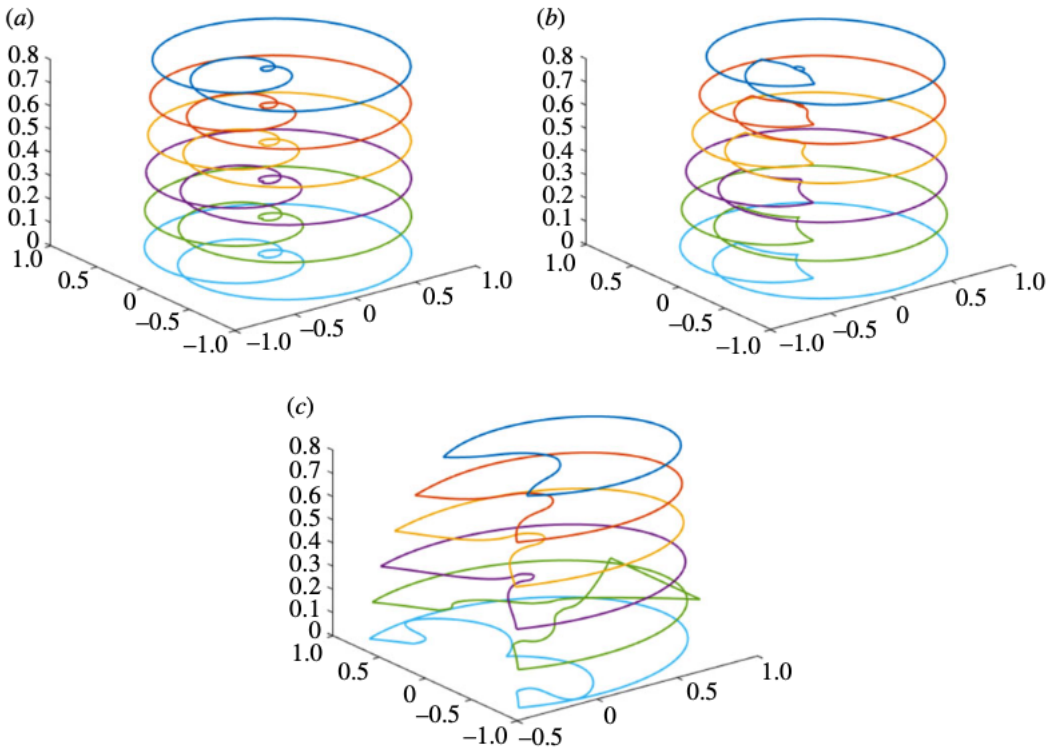

Figure 5. Evans function output for several Fourier frequencies $\xi \in [0, 0.8]$ on a semicircular contour with radius 0.4. (*a*) $\nu = 1/10$, (*b*) $\nu = 2/5$ and (*c*) $\nu = 8/5$. (Online version in colour.)

Evans contours can be seen to unwind from the origin, indicating that the eigenvalue pair has restabilized.

6. Conclusion

Computational Evans-function techniques are useful for a variety of purposes. First and foremost, because these techniques allow one to count the number of eigenvalues in the unstable complex half plane, they allow one to identify instabilities (e.g. [18]). Indeed, these computations can give insight into the nature of bifurcations (onset of instability), the ensuing dynamics and other behaviour. For example, evidence from Evans-function computations provided the impetus for the proof of stability in the strong-shock limit [50]. Additionally, because winding number counts can also rule out the possibility of unstable eigenvalues, the computational techniques described here can play a key role in determining spectral stability. These calculations are convincing when it is possible to rule out the possibility of large unstable eigenvalues through energy estimates [35, 42,77,78] or other analytical means [50,88]. In these analyses, the computational component is thus restricted to a finite part of the unstable half plane. Because it is often possible to prove a theorem to the effect that spectral stability implies nonlinear stability (in an appropriate sense), these calculations can provide convincing evidence of nonlinear stability. Indeed, these computations also provide the framework for numerical proofs of spectral stability [41]. Finally, we note that, as shown here, these techniques can be applied to physically relevant, multidimensional models for complex phenomena. The computations are naturally parallelizable, and this suggests that these computational Evans-function techniques are likely to be the major conduit for taking the large body of theoretical mathematical results about the stability of travelling waves and connecting it with meaningful applications.

Data accessibility. The numerical investigations in this paper were performed by via Stablab: a Matlab-based numerical library for Evans function computation [71]. The two examples examined in this paper are available in the repository.

Authors' contributions. The contributions of all of the authors are roughly equal. B.B., J.H. and G.L. developed the draft of the first four sections and J.L. drafted the final section, which is an outgrowth of his PhD dissertation. All four authors worked together with revisions. All authors read and approved the manuscript.

Competing interests. We declare we have no competing interests.

Funding. Research of the first author was supported in part by the US National Science Foundation under grant no. DMS-1400872. Research of the third author was supported in part by the US National Science Foundation under grant no. DMS-1413273.

Appendix A. Additional details for multidimensional detonation profiles

(a) Rescaling

The rescaling for the Navier–Stokes equations (5.1) is given below. Here, m is the constant value of the mass flux in the x-direction, and ϵ is chosen to normalize the density at the left end state to one. The simple equations of state used here are invariant under this scaling.

$$\left.\begin{aligned}&(x_1, x_2, t; \rho, u, v, T, z) \to \left(m x_1, m x_2, \epsilon m^2 t; \epsilon\rho, \frac{u}{\epsilon m}, \frac{v}{\epsilon m}, \frac{T}{\epsilon^2 m^2}, z\right)\\ \text{and}\qquad &\beta \to \frac{\beta}{\epsilon}, \quad q \to \frac{q}{\epsilon^2 m^2}, \quad k \to \frac{k}{\epsilon m^2}, \quad E_A \to \frac{E_A}{\epsilon^2 m^2}.\end{aligned}\right\} \tag{A 1}$$

(b) Travelling-wave equation

Let $\epsilon = 1/\rho_-$; then in the rescaled coordinates $\rho_- = u_- = 1$, $\hat{\rho}\hat{u} = 1$, and we obtain the system

$$u' + p' = (2\mu + \eta)u'', \tag{A 2a}$$

$$E' + (up)' = \frac{\kappa e''}{c_v} + (2\mu + \eta)(uu')' + qk\rho z\check{\varphi}(e) \tag{A 2b}$$

and

$$z' = (\rho\beta z')' - k\rho z\check{\varphi}(e). \tag{A 2c}$$

Substitute (A 2*c*) into (A 2*b*) to get

$$\begin{aligned} u' + p' &= (2\mu + \eta)u'', \\ E' + (up)' &= \frac{\kappa e''}{c_v} + (2\mu + \eta)(uu')' + q(\rho\beta z')' - qz', \\ z' &= (\rho\beta z')' - k\rho z\check{\varphi}(e). \end{aligned}$$

Integrating from $-\infty$ to x yields

$$(u - u_-) + (p - p_-) = (2\mu + \eta)u', \tag{A 3a}$$

$$(E - E_-) + (up - u_-p_-) = \frac{\kappa e'}{c_v} + (2\mu + \eta)uu' + q\rho\beta z' - q(z - z_-) \tag{A 3b}$$

and

$$z' = (\rho\beta z')' - k\rho z\check{\varphi}(e). \tag{A 3c}$$

Setting $\nu = \kappa/c_v$ and using $E = e + u^2/2$, we can substitute the first equation into the second to obtain

$$\begin{aligned} u' &= (2\mu + \eta)^{-1}((u - u_-) + (p - p_-)), \\ (e - e_-) - \frac{(u - u_-)^2}{2} &+ p_-(u - u_-) = \nu e' + q\rho\beta z' - q(z - z_-) \end{aligned}$$

and

$$z' = (\rho\beta z')' - k\rho z\check{\varphi}(e).$$

Since $u_- = \rho_- = z_- = 1$, after applying the pressure law $p = \Gamma\rho e$ the system becomes

$$\begin{aligned} u' &= (2\mu + \eta)^{-1}((u - 1) + \Gamma(\rho e - e_-)), \\ e' &= \nu^{-1}\left((e - e_-) - \frac{(u - 1)^2}{2} + \Gamma e_-(u - 1) - q\rho\beta z' + q(z - 1)\right) \end{aligned}$$

and

$$z' = (\rho\beta z')' - k\rho z\check{\varphi}(e).$$

From here, the final form reported in (5.4) follows immediately.

(c) Parametrization of end states

Solving (5.5*a*) for e_+ and substituting into (5.5*b*) allows us to parametrize e_+ and u_+ as functions of e_-, Γ and q, where

$$e_+ = u_+e_- + \Gamma^{-1}u_+(1 - u_+) \tag{A 4a}$$

and

$$u_+ = \frac{(\Gamma + 1)(\Gamma e_- + 1) - \sqrt{(\Gamma + 1)^2(\Gamma e_- + 1)^2 - \Gamma(\Gamma + 2)(1 + 2e_-(\Gamma + 1) + 2q)}}{\Gamma + 2}. \tag{A 4b}$$

The negative square root above is the parameter regime for strong detonations.

(d) The linearized eigenvalue equations

To be more concise, we write

$$\tilde{\mu} = (2\mu + \eta), \quad \tilde{\eta} = (\mu + \eta), \quad \hat{p} = \Gamma\hat{\rho}\hat{e}, \quad \gamma = \Gamma + 1.$$

The linearized eigenvalue problem comes from linearizing (5.2) about the travelling wave and taking the Fourier transform in the y-direction, resulting in

$$\lambda\rho + (\hat{\rho}u + \hat{u}\rho)' + \mathrm{i}\xi\hat{\rho}v = 0, \tag{A 5a}$$

$$\lambda(\hat{\rho}u + \hat{u}\rho) + (2u + \hat{u}^2\rho + \Gamma(\hat{e}\rho + \hat{\rho}e))' = \tilde{\mu}u'' - \xi^2\mu u + \mathrm{i}\xi(\tilde{\eta}v' - v), \tag{A 5b}$$

$$\lambda\hat{\rho}v + v' + \mathrm{i}\xi\Gamma(\hat{e}\rho + \hat{\rho}e) = \mu v'' - \xi^2\tilde{\mu}v + \mathrm{i}\xi\tilde{\eta}u', \tag{A 5c}$$

$$\begin{aligned}\lambda\left(\hat{\rho}e + u + \rho\left(\hat{e} + \frac{\hat{u}^2}{2}\right)\right) + \mathrm{i}\xi v\left(\gamma\hat{\rho}\hat{e} + \frac{\hat{u}}{2}\right) + \left[\gamma(\hat{e}\hat{u}\rho + e + \hat{e}\hat{\rho}u) + \frac{1}{2}\rho\hat{u}^3 + \frac{3}{2}\hat{u}u\right]' \\ = (ve' + \tilde{\mu}(\hat{u}'u + \hat{u}u') + \mathrm{i}\xi\eta\hat{u}v)' - \xi^2 ve \\ + \mu(\mathrm{i}\xi\hat{u}v' - \xi^2\hat{u}u) + \mathrm{i}\xi\eta\hat{u}_x v + qk(\hat{\rho}\hat{z}\breve{\varphi}'(\hat{e})e + \hat{\rho}\breve{\varphi}(\hat{e})z + \hat{z}\breve{\varphi}(\hat{e})\rho),\end{aligned} \tag{A 5d}$$

$$\begin{aligned}\lambda(\hat{z}\rho + \hat{\rho}z) + (\hat{u}\hat{z}\rho + \hat{\rho}\hat{z}u + z)' + \mathrm{i}\xi\hat{\rho}\hat{z}v \\ = \beta((\hat{\rho}z' + \hat{z}'\rho)' - \xi^2\hat{\rho}z) - k\big(\hat{\rho}\hat{z}\breve{\varphi}'(\hat{e})e + \hat{\rho}\breve{\varphi}(\hat{e})z + \hat{z}\breve{\varphi}(\hat{e})\rho\big).\end{aligned} \tag{A 5e}$$

We rewrite the system in flux coordinates, building off the work done in [88]; see also Barker *et al.* [66] for a more systematic derivation of flux variables and a discussion of their computational advantages. Defining flux variables

$$w_1 := -\hat{\rho}u - \hat{u}\rho, \tag{A 6a}$$

$$w_2 := \tilde{\mu}u' - (2u + \hat{u}^2\rho) - \Gamma(\hat{e}\rho + \hat{\rho}e) + \mathrm{i}\xi\tilde{\eta}v, \tag{A 6b}$$

$$w_3 := \mu v' - v + \mathrm{i}\xi\tilde{\eta}u, \tag{A 6c}$$

$$w_4 := \tilde{\mu}(\hat{u}_x u + \hat{u}u') + ve' - \gamma(e + \hat{u}\hat{e}\rho + \hat{e}\hat{\rho}u) - \left(\frac{3}{2}\hat{u}u + \frac{1}{2}\hat{u}^3\rho\right) + \mathrm{i}\xi\tilde{\eta}\hat{u}v \tag{A 6d}$$

and

$$w_5 := \beta(\hat{\rho}z' + \hat{z}_x\rho) - (\hat{u}\hat{z}\rho + \hat{\rho}\hat{z}u + z), \tag{A 6e}$$

we then adjust with

$$\tilde{w}_2 := w_2 - \hat{u}w_1 = \tilde{\mu}u' - u - \Gamma(\hat{e}\rho + \hat{\rho}e) + \mathrm{i}\xi\tilde{\eta}v \tag{A 7a}$$

and

$$\tilde{w}_4 := w_4 - \hat{u}\tilde{w}_2 - \hat{E}w_1 = ve' + \tilde{\mu}\hat{u}_x u - e - \hat{p}u. \tag{A 7b}$$

In this coordinate system, the eigenvalue equations become

$$w_1' = -\lambda\hat{\rho}w_1 - \lambda\hat{\rho}^2 u + \mathrm{i}\xi\hat{\rho}v, \tag{A 8a}$$

$$\tilde{w}_2' = -\hat{u}_x w_1 + (\lambda\hat{\rho} + \mu\xi^2)u, \tag{A 8b}$$

$$w_3' = -\mathrm{i}\xi\hat{p}w_1 - \mathrm{i}\xi\hat{p}\hat{\rho}u + (\lambda\hat{\rho} + \xi^2\tilde{\mu})v + \mathrm{i}\xi\Gamma\hat{\rho}e, \tag{A 8c}$$

$$\tilde{w}_4' = (-\hat{e}_x + \hat{z}f_2)w_1 - \hat{u}_x\tilde{w}_2 + \mathrm{i}\xi f_1(\hat{u}, \hat{u}_x)v \tag{A 8d}$$

$$+ f_4 e + \hat{\rho}\hat{z}f_2 u - f_2 z, \tag{A 8e}$$

$$w_5' = \mathrm{i}\xi\hat{\rho}\hat{z}v - \hat{\rho}\hat{z}f_3 w_1 - \hat{\rho}^2\hat{z}f_3 u + \hat{\rho}(\beta\xi^2 + f_3)z + k\hat{\rho}\hat{z}\breve{\varphi}'(\hat{e})e, \tag{A 8f}$$

$$\tilde{\mu}u' = -\hat{p}w_1 + \tilde{w}_2 + (1 - \hat{p}\hat{\rho})u - \mathrm{i}\xi\tilde{\eta}v + \Gamma\hat{\rho}e, \tag{A 8g}$$

$$\mu v' = w_3 - \mathrm{i}\xi\tilde{\eta}u + v, \tag{A 8h}$$

$$ve' = \tilde{w}_4 + (\hat{p} - \tilde{\mu}\hat{u}_x)u + e \tag{A 8i}$$

$$\beta z' = \hat{u}w_5 + \hat{u}z + \beta\hat{\rho}\hat{z}_x u + (\beta\hat{z}_x - \hat{u}\hat{z})w_1, \tag{A 8j}$$

where

$$f_1 = \hat{p} + (\mu - \eta)\hat{u}_x, \quad f_2 = qk\hat{\rho}\check{\varphi}(\hat{e}), \quad f_3 = \lambda + k\check{\varphi}(\hat{e}), \quad f_4 = \lambda\hat{\rho} + \nu\xi^2 - qk\hat{\rho}\hat{z}\check{\varphi}'(\hat{e}).$$

The 9×9 matrix A can be read off of this system.

References

1. Meshkov EE. 1969 Instability of the interface of two gases accelerated by a shock wave. *Fluid Dyn.* **4**, 101–104. (doi:10.1007/BF01015969)
2. Urtiew PA, Oppenheim AK. 1966 Experimental observations of the transition to detonation in an explosive gas. *Proc. R. Soc. Lond. A* **295**, 13–28. (doi:10.1098/rspa.1966.0223)
3. Torruellas WE, Wang Z, Hagan DJ, VanStryland EW, Stegeman GI, Torner L, Menyuk CR. 1995 Observation of two-dimensional spatial solitary waves in a quadratic medium. *Phys. Rev. Lett.* **74**, 5036–5039. (doi:10.1103/PhysRevLett.74.5036)
4. Davis RE, Acrivos A. 1967 Solitary internal waves in deep water. *J. Fluid Mech.* **29**, 593–607. (doi:10.1017/S0022112067001041)
5. Rauprich O, Matsushita M, Weijer CJ, Siegert F, Esipov SE, Shapiro JA. 1996 Periodic phenomena in proteus mirabilis swarm colony development. *J. Bacteriol.* **178**, 6525–6538. (doi:10.1128/jb.178.22.6525-6538.1996)
6. Niemela JJ, Ahlers G, Cannell DS. 1990 Localized traveling-wave states in binary-fluid convection. *Phys. Rev. Lett.* **64**, 1365–1368. (doi:10.1103/PhysRevLett.64.1365)
7. Durham AC, Ridgway EB. 1976 Control of chemotaxis in physarum polycephalum. *J. Cell. Biol.* **69**, 218–223. (doi:10.1083/jcb.69.1.218)
8. Evans JW. 1971/72 Nerve axon equations: I. Linear approximations. *Indiana Univ. Math. J.* **21**, 877–885. (doi:10.1512/iumj.1972.21.21071)
9. Evans JW. 1972/73 Nerve axon equations: II. Stability at rest. *Indiana Univ. Math. J.* **22**, 75–90. (doi:10.1512/iumj.1973.22.22009)
10. Evans JW. 1972/73 Nerve axon equations: III. Stability of the nerve impulse. *Indiana Univ. Math. J.* **22**, 577–593. (doi:10.1512/iumj.1973.22.22048)
11. Evans JW. 1974/75 Nerve axon equations: IV. The stable and the unstable impulse. *Indiana Univ. Math. J.* **24**, 1169–1190. (doi:10.1512/iumj.1975.24.24096)
12. Zumbrun K, Jenssen HK, Lyng G. 2005 Stability of large-amplitude shock waves of compressible Navier–Stokes equations. In *Handbook of mathematical fluid dynamics*, vol. 3 (eds S Friedlander, D Serre), pp. 311–533. Amsterdam, The Netherlands: North–Holland.
13. Sandstede B. 2002 Stability of travelling waves. In *Handbook of dynamical systems*, vol. 2 (ed. B Fiedler), pp. 983–1055. Amsterdam, The Netherlands: Elsevier Science.
14. Kapitula T, Promislow K. 2013 *Spectral and dynamical stability of nonlinear waves*. Applied Mathematical Sciences, vol. 185. New York, NY: Springer. With a foreword by Christopher K. R. T. Jones.
15. Alexander J, Gardner R, Jones C. 1990 A topological invariant arising in the stability analysis of travelling waves. *J. Reine Angew. Math.* **410**, 167–212. (doi:10.1515/crll.1990.410.167)
16. Humpherys J, Lyng G, Zumbrun K. 2009 Spectral stability of ideal-gas shock layers. *Arch. Ration. Mech. Anal.* **194**, 1029–1079. (doi:10.1007/s00205-008-0195-4)
17. Ghazaryan A, Humpherys J, Lytle J. 2013 Spectral behavior of combustion fronts with high exothermicity. *SIAM J. Appl. Math.* **73**, 422–437. (doi:10.1137/120864891)
18. Barker B, Humpherys J, Lyng G, Zumbrun K. 2015 Viscous hyperstabilization of detonation waves in one space dimension. *SIAM J. Appl. Math.* **75**, 885–906. (doi:10.1137/140980223)
19. Henry D 1981 *Geometric theory of semilinear parabolic equations*. Berlin, Germany: Springer.
20. Ghazaryan A, Latushkin Y, Schecter S. 2010 Stability of traveling waves for a class of reaction-diffusion systems that arise in chemical reaction models. *SIAM J. Math. Anal.* **42**, 2434–2472. (doi:10.1137/100786204)

21. Alexander JC, Sachs R. 1995 Linear instability of solitary waves of a Boussinesq-type equation: a computer assisted computation. *Nonlinear World* **2**, 471–507.
22. Gilbert F, Backus G. 1966 Propagator matrices in elastic wave and vibration problems. *Geophysics* **31**, 326–332. (doi:10.1190/1.1439771)
23. Ng BS, Reid WH. 1979 An initial value method for eigenvalue problems using compound matrices. *J. Comput. Phys.* **30**, 125–136. (doi:10.1016/0021-9991(79)90091-3)
24. Ng BS, Reid WH. 1979 A numerical method for linear two-point boundary value problems using compound matrices. *J. Comput. Phys.* **33**, 70–85. (doi:10.1016/0021-9991(79)90028-7)
25. Ng BS, Reid WH. 1980 On the numerical solution of the Orr-Sommerfeld problem: asymptotic initial conditions for shooting methods. *J. Comput. Phys.* **38**, 275–293. (doi:10.1016/0021-9991(80)90150-3)
26. Ng BS, Reid WH. 1985 The compound matrix method for ordinary differential systems. *J. Comput. Phys.* **58**, 209–228. (doi:10.1016/0021-9991(85)90177-9)
27. Brin LQ. 1998 Numerical testing of the stability of viscous shock waves. PhD thesis, Indiana University, Bloomington.
28. Brin LQ. 2001 Numerical testing of the stability of viscous shock waves. *Math. Comp.* **70**, 1071–1088. (doi:10.1090/S0025-5718-00-01237-0)
29. Brin LQ, Zumbrun K. 2002 Analytically varying eigenvectors and the stability of viscous shock waves. *Mat. Contemp.* **22**, 19–32. (Seventh Workshop on Partial Differential Equations, Part I (Rio de Janeiro, 2001).
30. Bridges TJ, Derks G, Gottwald G. 2002 Stability and instability of solitary waves of the fifth-order KdV equation: a numerical framework. *Physica D* **172**, 190–216. (doi:10.1016/S0167-2789(02)00655-3)
31. Allen L, Bridges TJ. 2002 Numerical exterior algebra and the compound matrix method. *Numer. Math.* **92**, 197–232. (doi:10.1007/s002110100365)
32. Humpherys J, Zumbrun K. 2006 An efficient shooting algorithm for Evans function calculations in large systems. *Physica D* **220**, 116–126. (doi:10.1016/j.physd.2006.07.003)
33. Drury LO. 1980 Numerical solution of Orr-Sommerfeld-type equations. *J. Comput. Phys.* **37**, 133–139. (doi:10.1016/0021-9991(80)90008-X)
34. Barker B, Freist&quote;uhler H, Zumbrun K. 2015 Convex entropy, Hopf bifurcation, and viscous and inviscid shock stability. *Arch. Rational Mech. Anal.* **217**, 309–372. (doi:10.1007/s00205-014-0838-6)
35. Humpherys J. 2009 On the shock wave spectrum for isentropic gas dynamics with capillarity. *J. Differ. Equ.* **246**, 2938–2957. (doi:10.1016/j.jde.2008.07.028)
36. Ledoux V, Malham SJA, Thümmler V. 2010 Grassmannian spectral shooting. *Math. Comp.* **79**, 1585–1619. (doi:10.1090/S0025-5718-10-02323-9)
37. Gesztesy F, Latushkin Y, Zumbrun K. 2008 Derivatives of (modified) Fredholm determinants and stability of standing and traveling waves. *J. Math. Pures Appl. (9)* **90**, 160–200. (doi:10.1016/j.matpur.2008.04.001)
38. Lafortune S, Lega J, Madrid S. 2011 Instability of local deformations of an elastic rod: numerical evaluation of the Evans function. *SIAM J. Appl. Math.* **71**, 1653–1672. (doi:10.1137/10081441X)
39. Barker B, Nguyen R, Sandstede B, Ventura N, Wahl C. 2017 Computing Evans functions numerically via boundary-value problems. (https://arxiv.org/abs/1710.02500)
40. Barker B, Johnson MA, Noble P, Rodrigues LM. 2013 Nonlinear modulational stability of periodic traveling-wave solutions of the generalized Kuramoto-Sivashinsky equation. *Physica D* **258**, 11–46. (doi:10.1016/j.physd.2013.04.011)
41. Barker B, Zumbrun K. 2016 Numerical proof of stability of viscous shock profiles. *Math. Models Methods Appl. Sci.* **26**, 1–19. (doi:10.1142/s0218202516500585)
42. Barker B, Humpherys J, Rudd K, Zumbrun K. 2008 Stability of viscous shocks in isentropic gas dynamics. *Comm. Math. Phys.* **281**, 231–249. (doi:10.1007/s00220-008-0487-4)
43. Coppel WA. 1978 *Dichotomies in stability theory*. Lecture Notes in Mathematics, vol. 629. Berlin, Germany: Springer.
44. Kapitula T, Sandstede B. 1998 Stability of bright solitary-wave solutions to perturbed nonlinear Schrödinger equations. *Physica D* **124**, 58–103. (doi:10.1016/S0167-2789(98)00172-9)
45. Gardner RA, Zumbrun K. 1998 The gap lemma and geometric criteria for instability of viscous shock profiles. *Comm. Pure Appl. Math.* **51**, 797–855. (doi:10.1002/(SICI)1097-0312(199807)51:7<797::AID-CPA3>3.0.CO;2-1)

46. Benzoni-Gavage S, Serre D, Zumbrun K. 2001 Alternate Evans functions and viscous shock waves. *SIAM J. Math. Anal.* **32**, 929–962 (electronic). (doi:10.1137/S0036141099361834)
47. Bader G, Ascher U. 1987 A new basis implementation for a mixed order boundary value ode solver. *SIAM J. Sci. Stat. Comput.* **8**, 483–500. (doi:10.1137/0908047)
48. Doedel E, Champneys A, Fairgrieve T, Kuznetsov Y, Sandstede B, Wang X. 2009 Auto97: Continuation and bifurcation software for ordinary differential equations. (https://www.researchgate.net/publication/259563149)
49. Hale N, Moore DR. 2008 A sixth-order extension to the MATLAB package bvp4c of J. Kierzenka and L. Shampine. Technical Report NA-08/04, Oxford University Computing Laboratory.
50. Humpherys J, Lafitte O, Zumbrun K. 2010 Stability of isentropic Navier-Stokes shocks in the high-Mach number limit. *Comm. Math. Phys.* **293**, 1–36. (doi:10.1007/s00220-009-0885-2)
51. Davey A. 1983 An automatic orthonormalization method for solving stiff boundary value problems. *J. Comput. Phys.* **51**, 343–356. (doi:10.1016/0021-9991(83)90098-0)
52. Dieci L, Russell RD, Van Vleck ES. 1994 Unitary integrators and applications to continuous orthonormalization techniques. *SIAM J. Numer. Anal.* **31**, 261–281. (doi:10.1137/0731014)
53. Dieci L, Van Vleck ES. 2000 Continuous orthonormalization for linear two-point boundary value problems revisited. In *Dynamics of algorithms (Minneapolis, MN, 1997)*, pp. 69–90. IMA Vol. Math. Appl., vol. 118. New York, NY: Springer.
54. Dieci L, Van Vleck ES. 2003 Orthonormal integrators based on householder and givens transformations. *Future Gener. Comput. Syst.* **19**, 363–373. (doi:10.1016/S0167-739X(02)00163-2)
55. Dieci L, Van Vleck ES. 2008 On the error in QR integration. *SIAM J. Numer. Anal.* **46**, 1166–1189. (doi:10.1137/06067818X)
56. Ascher UM, Chin H, Reich S. 1994 Stabilization of DAEs and invariant manifolds. *Numer. Math.* **67**, 131–149. (doi:10.1007/s002110050020)
57. Higham DJ. 1997 Time-stepping and preserving orthonormality. *BIT* **37**, 24–36.
58. Bindel D, Demmel J, Friedman M. 2008 Continuation of invariant subspaces in large bifurcation problems. *SIAM J. Sci. Comput.* **30**, 637–656. (doi:10.1137/060654219)
59. Dieci L, Elia C, Van Vleck E. 2010 Exponential dichotomy on the real line: SVD and QR methods. *J. Differ. Equ.* **248**, 287–308. (doi:10.1016/j.jde.2009.07.004)
60. Dieci L, Elia C, Van Vleck E. 2011 Detecting exponential dichotomy on the real line: SVD and QR algorithms. *BIT* **51**, 555–579. (doi:10.1007/s10543-010-0306-0)
61. Zumbrun K. 2009 Numerical error analysis for Evans function computations: a numerical gap lemma, centered-coordinate methods, and the unreasonable effectiveness of continuous orthogonalization. Preprint, arXiv:0904.0268.
62. Kato T. 1995 *Perturbation theory for linear operators*. Classics in Mathematics. Berlin, Germany: Springer. Reprint of the 1980 edition.
63. Humpherys J, Sandstede B, Zumbrun K. 2006 Efficient computation of analytic bases in Evans function analysis of large systems. *Numer. Math.* **103**, 631–642. (doi:10.1007/s00211-006-0004-7)
64. Zumbrun K. 2010 A local greedy algorithm and higher-order extensions for global numerical continuation of analytically varying subspaces. *Quart. Appl. Math.* **68**, 557–561. (doi:10.1090/S0033-569X-2010-01209-1)
65. Sattinger DH. 1976 On the stability of waves of nonlinear parabolic systems. *Adv. Math.* **22**, 312–355. (doi:10.1016/0001-8708(76)90098-0)
66. Barker B, Humpherys J, Lyng GD, Zumbrun K. 2017 Balanced flux formulations for multidimensional Evans function computations for viscous shocks. Preprint, arxiv:1703.02099.
67. Gubernov V, Mercer GN, Sidhu HS, Weber RO. 2003 Evans function stability of combustion waves. *SIAM J. Appl. Math.* **63**, 1259–1275. (doi:10.1137/S0036139901400240)
68. Barker B. 2009 Evans function computation. Master's thesis, Brigham Young University, Provo.
69. Bronski JC. 1996 Semiclassical eigenvalue distribution of the Zakharov-Shabat eigenvalue problem. *Physica D* **97**, 376–397. (doi:10.1016/0167-2789(95)00311-8)
70. Humpherys J, Lytle J. 2015 Root following in Evans function computation. *SIAM J. Numer. Anal.* **53**, 2329–2346. (doi:10.1137/140975590)

71. Barker B, Humpherys J, Lytle J, Zumbrun K. June 2015 STABLAB: a MATLAB-based numerical library for Evans function computation. Available in the github repository, http://github.com/nonlinear-waves/stablab/.
72. Courant R, Friedrichs KO. 1976 *Supersonic flow and shock waves*. New York, NY: Springer.
73. Erpenbeck JJ. 1962 Stability of steady-state equilibrium detonations. *Phys. Fluids* **5**, 604–614. (doi:10.1063/1.1706664)
74. Lee HI, Stewart DS. 1990 Calculation of linear detonation instability: one-dimensional instability of plane detonation. *J. Fluid Mech.* **216**, 103–132. (doi:10.1017/S0022112090000362)
75. Powers JM, Paolucci S. 2005 Accurate spatial resolution estimates for reactive supersonic flow with detailed chemistry. *AIAA J.* **43**, 1088–1099. (doi:10.2514/1.11641)
76. Majda A. 1981 A qualitative model for dynamic combustion. *SIAM J. Appl. Math.* **41**, 70–93. (doi:10.1137/0141006)
77. Humpherys J, Lyng G, Zumbrun K. 2013 Stability of viscous detonations for Majda's model. *Physica D* **259**, 63–80. (doi:10.1016/j.physd.2013.06.001)
78. Hendricks J, Humpherys J, Lyng G, Zumbrun K. 2015 Stability of viscous weak detonation waves for Majda's model. *J. Dyn. Diff. Equ.* **27**, 237–260. (doi:10.1007/s10884-015-9440-3)
79. Faria LM, Kasimov AR, Rosales RR. 2014 Study of a model equation in detonation theory. *SIAM. J. Appl. Math.* **74**, 547–570. (doi:10.1137/130938232)
80. Gardner RA. 1983 On the detonation of a combustible gas. *Trans. Am. Math. Soc.* **277**, 431–468. (doi:10.1090/S0002-9947-1983-0694370-1)
81. Gasser I, Szmolyan P. 1993 A geometric singular perturbation analysis of detonation and deflagration waves. *SIAM J. Math. Anal.* **24**, 968–986. (doi:10.1137/0524058)
82. Lyng G, Zumbrun K. 2004 One-dimensional stability of viscous strong detonation waves. *Arch. Ration. Mech. Anal.* **173**, 213–277. (doi:10.1007/s00205-004-0317-6)
83. Lyng G, Zumbrun K. 2004 A stability index for detonation waves in Majda's model for reacting flow. *Physica D* **194**, 1–29. (doi:10.1016/j.physd.2004.01.036)
84. Jenssen HK, Lyng G, Williams M. 2005 Equivalence of low-frequency stability conditions for multidimensional detonations in three models of combustion. *Indiana Univ. Math. J.* **54**, 1–64. (doi:10.1512/iumj.2005.54.2685)
85. Costanzino N, Jenssen HK, Lyng G, Williams M. 2007 Existence and stability of curved multidimensional detonation fronts. *Indiana Univ. Math. J.* **56**, 1405–1461. (doi:10.1512/iumj.2007.56.2972)
86. Lyng G, Raoofi M, Texier B, Zumbrun K. 2007 Pointwise Green function bounds and stability of combustion waves. *J. Diff. Equ.* **233**, 654–698. (doi:10.1016/j.jde.2006.10.006)
87. Barker B, Humpherys J, Lyng G, Zumbrun K. 2017 Euler vs. lagrange: the role of coordinates in practical Evans-function computations. (https://arxiv.org/abs/1707.01938)
88. Humpherys J, Lyng G, Zumbrun K. 2017 Multidimensional stability of large-amplitude Navier–Stokes shocks. *Arch. Ration. Mech. Anal.* **226**, 923–973. (doi:10.1007/s00205-017-1147-7)